Optimizing the energy performance of industrial refrigeration plants using digital twins

Animesh Sahoo

TU Delft

GEA

Optimizing the energy performance of industrial refrigeration plants using digital twins

by

Animesh Sahoo

to obtain the degree of Master of Science in Mechanical Engineering

specializing in Energy, Flow & Process Technology

at the Delft University of Technology,

to be defended publicly on Friday June 16, 2023 at 10:30 AM.

Student number:	5426618	
Project duration:	October 17, 2022 – June 16, 2023	
Thesis committee:	Prof. dr. ir. C. A. Infante Ferreira,	TU Delft, supervisor
	Prof. dr. ir. K. Hooman,	TU Delft, Chair
	Prof. dr. ir. M. Ramdin,	TU Delft

TU Delft

Abstract

Industrial refrigeration systems are known to consume approximately 17% of electrical energy, a figure that is projected to rise in the future. This high energy consumption contributes to global warming and environmental degradation since conventional sources of energy are typically utilized for electricity generation. Moreover, the energy-intensive nature of industrial refrigeration systems leads to increased costs for major food and beverage industries. Consequently, optimizing the energy efficiency of these systems becomes crucial.

In this research, the application of Digital Twin (DT) technologies was explored, which have demonstrated effectiveness in various areas such as supply chain streamlining and system optimization. By combining physical and virtual spaces, DT and big data analytics can facilitate energy performance evaluation and optimization. The literature review identified three categories of DT models: physics-based, empirical, and data-driven. Considering their accuracy and efficiency, empirical models were recommended for developing DT models, while data-driven models proved useful for performance prediction applications. It was recommended to establish empirical equations based on correlation analysis by adjusting higher degree terms for accuracy. Additionally, input-output parameters for the DT should be tailored to the specific application and equipment. The literature study showed the possible identification of energy performance deviations, their root causes, and potential optimizations, including equipment optimization, load sharing among parallel equipment, and optimization of condenser set points and defrosting time.

This thesis research focuses on three industrial refrigeration plants: the Verkade Plant, the LST Plant, and the GIST Plant. For the Verkade Plant, empirical models were developed and validated for the screw compressor, evaporator, and evaporative condenser. An algorithm for condenser optimization was proposed and tested, while deviations in evaporator performance were analyzed. Similar models were developed and validated for the LST and GIST Plants, enabling the prediction of equipment performance. The predicted results were compared to actual plant performance, and deviations were carefully examined. Furthermore, optimization techniques were applied to improve equipment efficiency.

The thesis research findings indicate that the empirical models for each equipment piece at the Verkade Plant achieved an accuracy within a 5% error range, suggesting their suitability for analyzing the other two plants. The proposed condenser optimization algorithm has the potential to annually save 7% of energy, resulting in savings of 32 MWh of electrical energy and 11 tonnes of CO_2 emissions. The application of the proposed optimization techniques to the LST and GIST Plant resulted in a significant reduction in energy consumption. It was determined that these techniques can achieve savings of approximately 13% and 14% in total energy consumption, corresponding to 200 MWh and 170 MWh of electrical energy, as well as 70 tonnes and 60 tonnes of CO_2 emissions, respectively. These energy savings contribute to the reduction of CO_2 released into the atmosphere, aligning with the goals of the Paris Agreement. Consequently, this research offers valuable insights into mitigating global warming through the optimization of industrial refrigeration systems using DT technology.

Animesh Sahoo
Delft, June 2023

Contents

Nomenclature

Acronyms

AI	Artificial intelligence
ANN	Artificial neural network
DT	Digital twin
EER	Energy efficiency ratio
GBR	Gradient booster regression
GWP	Global warming potential
ML	Machine learning
MSE	Mean square error
ODP	Ozone depletion potential
PID	Piping & instrumentation diagram
RMS	Root mean square
SVM	Support vector machine
SVR	Support vector regression
VFD	Variable frequency drive

Greek Symbols

Δ	Difference	
ρ	Density	kg/m^3

Roman Symbols

C	Capacity	kW
cf	Capacity factor	
cp	Specific heat capacity	J/kgK
D	Diameter	m
DBT	Dry bulb temperature	K
E	Energy	J
FS	Fan speed	m/s
$\dot{m}$	Mass flow rate	kg/s
N	Rotational speed	RPM
P	Power	kW

p	Pressure	Pa
T	Temperature	K
WBT	Wet bulb temperature	K
Z	Valve opening	

Subscripts

air	Air
$comp$	Compressor
$cond$	Condenser
$cool$	Cooling
$curr$	Current
$evap$	Evaporator
gly	Glycol
in	Inlet
nom	Nominal
out	Outlet
rat	Rated
ref	Refrigerant
suc	Suction
wat	Water

1

Introduction

1.1. Research background

As per Outlook (2019), by 2040 global energy consumption is expected to increase by 50%. Globally 40% of total energy consumption and CO_2 emissions are attributed to buildings (Moran et al. (2017)). Industrial refrigeration systems currently account for 17% of total electric energy consumption, with projections indicating a 30% increase by 2050 (Ahmed et al. (2021)). In urban cities, refrigeration and air conditioning contribute to 50-60% of the total electrical energy consumption, and 80% of this electrical energy is associated with conventional energy sources (Solomon et al. (2007)). This reliance on conventional energy sources leads to greenhouse gas emissions and global warming, particularly due to refrigerant leakage and gas emissions associated with these systems (McMullan (2002)). The leakage of high-ODP and high-GWP refrigerants have detrimental effects on the environment. Even with the use of low-ODP and low-GWP refrigerants, sub-optimal operation and inadequate performance result in higher energy consumption (Ahmed et al. (2021)).

The industrial refrigeration system has a significant societal impact as it is extensively used in the food and beverage industries for various applications. Optimizing the energy performance of these systems can reduce the cost of consumables and redirect the saved energy for domestic purposes, contributing to a more sustainable future. In the context of climate change, it is imperative for energy-consuming industries to improve their energy performance to mitigate the adverse effects of global warming.

Refrigeration is a highly energy-intensive process, particularly in sectors such as chemical, petrochemical, food, and pharmaceuticals. In some cold storage facilities, these systems can account for up to 90% of the total energy consumption (Dincer et al. (2017)). Therefore, optimizing these systems becomes crucial to reduce operational costs. Additionally, governments are striving to meet the goals of the Paris Agreement by reducing CO_2 emissions by 45% (Gurubalan et al. (2019)). Consequently, minimizing the energy consumption of refrigeration systems is critical to mitigate global warming and comply with international climate commitments.

Various strategies are employed to reduce the emissions, like increasing the efficiency of the energy technology, utilizing alternative energy sources, and capturing CO_2 emissions. Efficiency can be increased in various ways/stages like design, operation, and equipment selection. In this thesis, emphasis is given to increasing the energy efficiency of industrial refrigeration systems during the operation stage.

Smart manufacturing has gained prominence in modern manufacturing industries, leveraging advanced sensors, data transmission, and collection to gather data. Big data analytics are then used for failure analysis, streamlining the supply chain, optimizing production, and reducing energy con-

sumption. But the major challenge in smart manufacturing is the integration of physical and virtual spaces, which is where digital twins (DTs) play a crucial role. DTs merge physical and virtual environments, facilitating the analysis of physical technologies in a virtual space. DTs have been successfully implemented across a wide range of industries and are also applied in refrigeration systems for the optimization of system components, failure detection, fault diagnosis, and defrosting optimization. Hence, DT and industrial data should be used for energy performance evaluation and optimization (Tao et al. (2018)).
As identified in the literature review, there could be possible discrepancies between the actual and predicted performance of equipment. Therefore, it is crucial to thoroughly assess the underlying factors contributing to these deviations and address them prior to optimizing the system. Furthermore, it is imperative to compare the energy savings achieved before and after the optimization process to ascertain the economic viability of implementing the proposed optimization strategies in refrigeration systems. Quantifying the energy savings will also facilitate the assessment of the corresponding reduction in atmospheric CO_2 levels.

1.2. Definition & terminologies

1.2.1. Digital twin (DT)

A DT is a virtual representation of a physical entity or process. DTs are usually related to the physical twin through some unique characteristics that identify the physical twin (Rios et al. (2015), Kiritsis (2011)). Hence, a bijective relation exists between the twins. The DT follows the lifecycle of its physical twin, hence it can be used for monitoring, controlling, and optimizing processes and functions. Moreover, it can predict future statuses, which in turn can be used for predictive maintenance. Due to the advancement in big data storage capabilities, real-time data from the physical twin can be collected and used immediately. This helps the DT to be synchronized with the physical world at all times. With the help of empirical or data-based algorithms, it is used for continuous optimization of the process (Barricelli et al. (2019)).
The modeling of DT consists of three stages. First is the design stage, where out of numerous modeling techniques available, a suitable technique is decided based on the application. After a suitable technique is decided, in the second stage coding is done using to develop a virtual twin of the physical entity or process. The last stage is validation and operation, where the model is validated using test data to check if it is within the defined error tolerance. Finally, it is used for the desired application.
In the literature research (Sahoo (2023)), the available modeling techniques were reviewed based on various parameters and a suitable technique was selected for energy performance evaluation. The equations and input-output parameters used for modeling were also reviewed and listed. The same was used for this thesis research.

1.2.2. Machine learning (ML)

Artificial intelligence (AI) is human intelligence being exhibited by machines. With the advancement of technology, there has been increase in large data sets ("big data"). AI is used for evaluating big data to extract information from it, which is used for numerous applications.
ML is a subset of AI that is capable of experiential learning like human beings. Computational algorithms are used for ML to learn and improve its analyses. The algorithms use a large set of data to learn the input-output pattern to make autonomous decisions. With sufficient data, the machine can predict an output from the given input. In order to improve the model, outputs are usually compared with the actual data and then suitable corrections are made (Helm et al. (2020)).
Various ML techniques are available based on the application. ML techniques are subdivided into

two categories classification and regression models. For this thesis, four regression models were used for energy performance evaluation. Mostly for energy performance calculation regression models and Artificial Neural Networks (ANN) are used.

Polynomial regression

Polynomial regression is a popular regression technique that models the relationship between the independent variable and the dependent variable as an nth-degree polynomial. It extends the linear regression model by introducing higher-order terms, allowing for nonlinear relationships to be captured. The model fits a curve that best represents the data points, providing a flexible approach to handle complex data patterns. Polynomial regression has been successfully applied in various fields such as economics, physics, and social sciences (Draper (1966)).

Support vector regression (SVR)

Support vector regression is a powerful regression technique that uses support vector machines (SVMs) to model the relationship between variables. SVR aims to find a hyperplane in a high-dimensional feature space that best fits the data points while maintaining a minimum margin of error. By mapping the data into a higher-dimensional space, SVR can handle nonlinear relationships and outliers effectively. It has been successfully applied in various domains, including finance, engineering, and bioinformatics (Smola and Schölkopf (2004)).

Gradient boosting regression (GBR)

Gradient boosting regression is an ensemble method that combines multiple weak predictive models, typically decision trees, to create a strong predictive model. It builds the model iteratively by adding new trees that focus on the residuals of the previous models, gradually reducing the prediction error. Gradient boosting regression excels at handling complex data patterns and capturing nonlinear relationships. It has achieved remarkable success in various applications, such as predicting housing prices, customer churn, and stock market trends (Friedman (2001)).

Random forest regression

Random forest regression is another ensemble technique that utilizes multiple decision trees to make predictions. It constructs a collection of decision trees using bootstrapped samples of the data and randomly selecting subsets of features at each split. The final prediction is obtained by averaging the predictions of individual trees. Random forest regression can handle high-dimensional data, capture complex interactions, and handle missing values effectively. It has found applications in various domains, including healthcare, finance, and ecology (Breiman (2001)).

Artificial neural network (ANN)

ANN is a computational method to solve complex problems. It behaves like a black box that has outputs for a set of inputs. It is mostly used for data-driven models. It consists of three layers input, output, and hidden layers, where the number of hidden layers depends on the application. Neurons are the basic components of ANN. They are present in each layer and they receive signals from other neurons to produce a single output. The output of neurons is based on sigmoid functions. Based on the weightage of neurons, final outputs are obtained. The data used for ANN is divided into two sets, training, and test data. The training data is used to train the model and the test data is used to validate the model (Belman-Flores et al. (2017)).

1.3. Research objectives

The goals for the thesis research are:

- to develop DTs for each type of equipment using the modeling technique, equations, input, and output parameters defined in the literature
- to evaluate the energy performance of each piece of equipment using the parameters defined in the literature
- to compare the energy performance of the DT with actual site data and to check for deviation in performance
- to identify the root cause of the deviation (if any) and to correct the digital twin accordingly
- to optimize the refrigeration system set points and to minimize energy consumption during operation
- to optimize the defrosting and load sharing
- to calculate the energy savings

1.4. Methodology

Figure 1.1 refers to the methodology to be used for this thesis research. The research background was presented, highlighting the significance of the study from various perspectives. That led to the formulation of research questions, which subsequently defined the objectives of the thesis research. Three industrial plants, namely the Verkade plant, the LST plant, and the GIST plant, were selected for analysis. Prior to analysis, actual plant data were collected for each plant and carefully examined for errors. Any identified errors were subsequently eliminated. Experimental data relevant to the equipment being analyzed was also collected. Digital twin (DT) models were developed and validated for each piece of equipment using the equipment data sheet and the collected experimental data. Validation ensured the accuracy and reliability of the DT models. The validated DT models were employed to predict the performance of the equipment based on the actual plant data. These predicted performance values were then compared against the actual performance of the equipment. Deviations between predicted and actual performance were thoroughly evaluated to identify the root causes. In cases where deviations between predicted and actual performance were observed, a detailed analysis was conducted to identify the factors contributing to these discrepancies. Conversely, if no deviations were found, the equipment was assessed for potential energy performance improvements. When opportunities for energy performance improvement were identified, an appropriate optimization algorithm was developed to exploit these opportunities. The algorithm was designed to optimize energy consumption and enhance overall performance. The proposed optimization algorithm was applied to estimate the energy savings achievable through its implementation. Quantitative analysis was performed to assess the impact of the algorithm on energy efficiency. Conclusions and discussions were presented, summarizing the findings of the thesis research in relation to the defined research objectives. The implications of the results were discussed, along with any limitations or constraints encountered during the study. Recommendations were provided for future research endeavors, highlighting potential areas of investigation and suggesting avenues for expanding upon the current study.

1.5. Report Structure

Chapter 1 consists of the research background which explains why this particular thesis research is being performed. It is followed by an explanation of the concepts of digital twins, machine learning, and some of the machine learning techniques used in the thesis. The thesis research objectives are enlisted that will be answered through this thesis. Subsequently, a step-by-step method that will be followed throughout the thesis research is explained. Lastly, the report structure is explained.

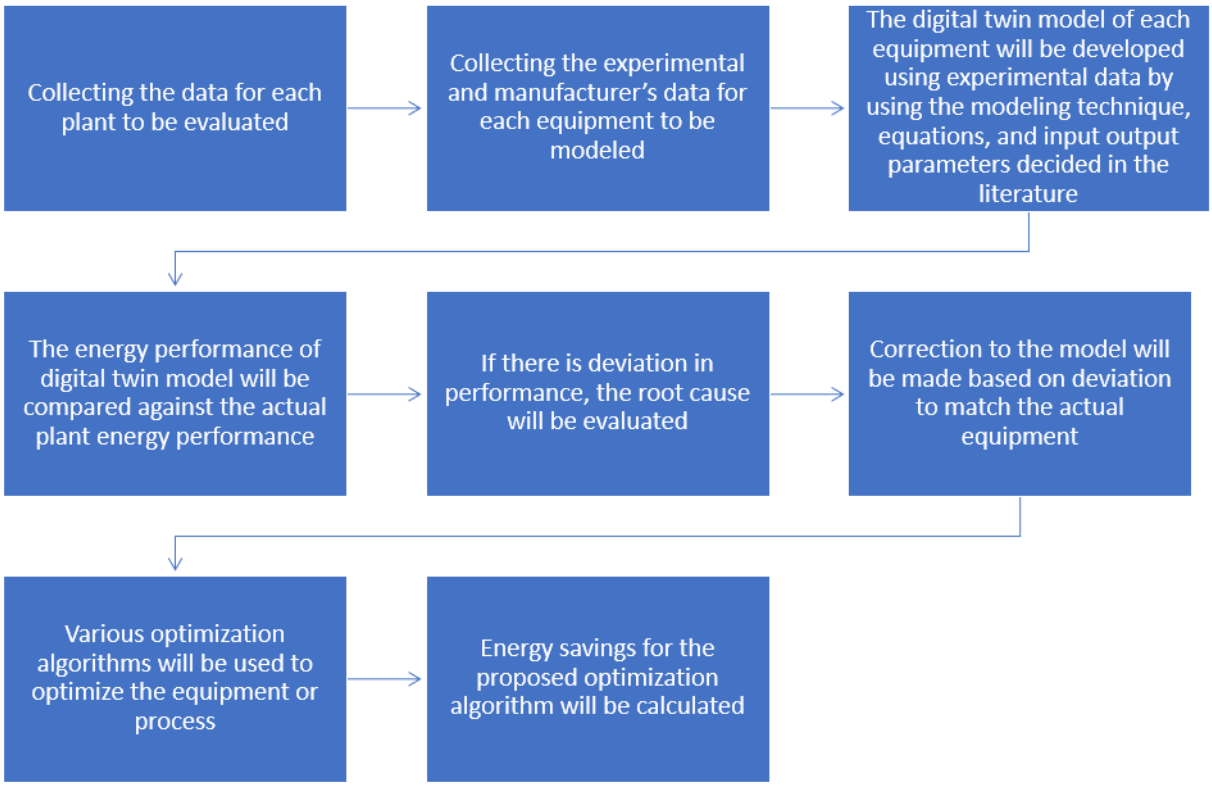

Figure 1.1: Methodology for thesis research

Chapter 2 consists of literature findings. It summarizes the main findings and conclusions of the literature review that are relevant to this thesis research.
Chapter 3 consists of the Verkade plant analysis. First, the system details of the plant are described. Followed by the description of the digital twin models of the compressor, evaporative condenser, and evaporator along with their validation. The comparison of predicted and actual performance is reported. The optimization of the condenser set point is explained. Finally, conclusions from the plant analysis are summarized.
Chapter 4 consists of the LST plant analysis. Similar to the Verkade plant analysis, first the system details are explained. That is followed by the screw compressor analysis. Detailed analysis results are reported which include model validation, parallel operation optimization, energy savings, and behavior of the model at startup. Subsequently, the evaporative condenser model analysis is described. The deviation in behavior, root cause analysis, set point optimization, and energy savings are reported. Further, expansion valve and evaporator models are described along with their analysis. Finally, the conclusions from the LST plant are discussed.
Chapter 5 consists of the GIST plant analysis. First, the system details are described. It is followed by the screw compressor (within the chiller) analysis. The analysis includes modeling, validation, optimization, and energy savings calculation. Subsequently, the evaporator and condenser (within the chiller) are analyzed. The root cause analysis of deviation in condenser performance is reported. Then the hybrid cooler is analyzed. The limitations in the availability of experimental data leading to the development of an unreliable model are explained. Following that air-cooler model and defrosting operations are analyzed and reported. Finally, the conclusions from the GIST plant are discussed.
Chapter 6 presents the overall conclusion from the thesis along with the research answers and their discussion. The limitations and recommendations for further study are provided.

2

Literature Findings & Conclusions

The following was concluded from the literature study:

- Three types of DT models were identified during the literature review (Sahoo (2023)), they are physics-based, empirical, and data-driven models. Physics-based models have twice the computation time as compared to data-driven models. Hence, physics-based models should be eliminated as higher computation time leads to higher costs of computation. Industrial refrigeration plants usually generate billions of data in a year, hence, computation time is a significant factor.
- Based on the accuracy of the model, empirical models were found to be more accurate than the data-driven models as they have a lower error percentage for performance evaluation. Accurate models help in recognizing the deviation in performance with ease. Hence, empirical models should be used for energy performance evaluation. However, reliable equipment performance data sets are required to develop the empirical models. These data sets can be provided by the manufacturers and GEA.
- The time spent to develop the models and reusability of a single model for different scaling is important for the model selection because higher model development time leads to higher cost and reusability of the model can save time.
- Based on the applications, it was observed that data-driven models have been widely used for performance prediction applications. Artificial Neural Network (ANN) was found to be the most accurate data-driven model. Hence, for optimization, both data-driven and empirical models should be used to check which one gives the better result.
- For developing the empirical DT models various equations were used by different researchers. It was observed that the equations were similar with a variation in higher degree terms and coefficients. The similarity in equations was due to the correlation analysis which gives a similar correlation for similar equipment. However, the variation in higher degree terms and coefficients were due to the accuracy and data used for the development of DT models. Hence, similar equations should be used for the empirical DT models with different higher-degree terms and coefficients based on the defined accuracy of the model and data used for its development (refer to equations 2.1 to 2.7).
- It was observed that various input-output parameters were used in the DT models based on the application and equipment type. Hence, the input-output parameters that should be used

to model the DTs are listed in table 2.1. These parameters are based on the equipment to be evaluated, availability of data, and energy performance evaluation application.

- Some deviations in energy performance were listed along with their root cause (refer to table 2.2). These deviations were found by the authors during the energy performance evaluation for different equipment using DT models. If the same deviation is found in the energy performance evaluation during this thesis, the probable causes should be taken into consideration.
- For optimization, first the part load behaviors of the equipment were studied. It was observed that at part load the reciprocating compressors had better performance in comparison to screw compressors. Hence, when the reciprocating compressors are running in parallel, the load should be split equally. For screw compressors running in parallel, the load should be split equally when the loads are above 100% and below that one of the compressors should be fully loaded.
- It was observed that the optimizations were divided into high and low-pressure side optimization. For the high-pressure side, condenser fan speed optimization was performed using various algorithms to find the minimum power consumption for the compressor and the condenser fan combined. Hence, the condenser set point should be optimized by minimizing the power consumption for the condenser fan and the compressor.
- For the low-pressure side, the defrosting optimization was performed by different techniques. Refrigerant inlet temperature, the interval for defrosting, and the mass flow rate of refrigerant were some of the parameters optimized. However, the mass flow rate does not change much during defrosting, so, the focus should be on defrosting time and inlet pressure. The defrosting optimization should be performed using the energy trade-off between the energy penalty due to frosting and energy consumption due to defrosting.
- For the low-pressure side, the cooling load was managed to optimize the energy consumption. The load modulation should be done by switching off the evaporators in the different refrigerated spaces without compromising the product stored.

The following are the equations reported in the literature review that are used to develop the equipment DT models. Equations 2.1 and 2.2 are used to calculate the compressor cooling capacity and power consumption respectively. While equations 2.3 to 2.7 are used to calculate condensing capacity of the condenser.

$$\begin{aligned} C_{cool,comp} =& C_1 + C_2 \times T_{evap} + C_3 \times T_{cond} + C_4 \times T_{cond}^2 + C_5 \times T_{evap} \times T_{cond} + C_6 \times T_{cond}^2 \\ &+ C_7 \times T_{cond} \times T_{evap}^2 + C_8 \times T_{cond}^2 \times T_{evap} + C_9 \times T_{cond}^2 \times T_{evap}^2 \end{aligned} \tag{2.1}$$

where,
$C_n = coefficients\, calculated\, using\, experimental\, data$

$$\begin{aligned} P_{comp} =& P_1 + P_2 \times T_{evap} + P_3 \times T_{cond} + P_4 \times T_{cond}^2 + P_5 \times T_{evap} \times T_{cond} + P_6 \times T_{cond}^2 \\ &+ P_7 \times T_{cond} \times T_{evap}^2 + P_8 \times T_{cond}^2 \times T_{evap} + P_9 \times T_{cond}^2 \times T_{evap}^2 \end{aligned} \tag{2.2}$$

where,
$P_n = coefficients\, calculated\, using\, experimental\, data$

$$C_{cond,nom} = C_{rat} \cdot cf \tag{2.3}$$

$$F_2 = (FS\%)^3 \tag{2.4}$$

$$F_1 = (F_2)^{0.17} \tag{2.5}$$

$$C_{cond,nom,curr} = F_1 \cdot C_{cond,nom} \tag{2.6}$$

$$cf_{curr} = \frac{C_{cond,nom,curr}}{C_{cond,curr}} \tag{2.7}$$

Table 2.1: Summary of input & output parameters to be used in this thesis

Equipment	**Input/measured values**	**Fixed/known values**	**Output**
Reciprocating compressor	T_{evap}, T_{cond}, N, number of cylinders activated	Polynomial coefficients	P_{comp}, C_{comp}
Screw compressor	T_{evap}, T_{cond}, N, slide valve position	Polynomial coefficients	P_{comp}, C_{comp}
Air-cooled condenser*	$DBT, T_{cond}, FS\%$	$C_{cond,rat}$	C_{cond}
Evaporative condenser*	$T_{cond}, FS\%, WBT$	$C_{cond,rat}, cf$ table	C_{cond}
Air cooler	$C_{comp}\#, T_{air,in}, p_{ref,out}$		ΔT_{out}
Liquid cooler	$C_{comp}\#, T_{wat,out}, p_{ref,out}$		ΔT_{out}
Valve	$p_{in}, p_{out}, D, \rho, Z$, non-dimensional coefficients		$\dot{m}$

*** Each of $FS\%$, C_{cond}, T_{cond} can be calculated when other two parameters are known.**
 # Calculated value

Table 2.2: Summary of deviations and their possible causes

Possible effects/measured deviations	Possible causes	References
Failure to minimise the heat load*	poor control of doors on the system*	Pearson (2019)
	poor maintenance of the building fabric*	Pearson (2019)
	poor control of incoming product temperature*	Pearson (2019), Cobo and Renilla (2015)
	insufficient charge	Goswami et al. (1997), Choi and Kim (2002), Cho et al. (2005), Farzad (1990)
Poor compressor control	several fixed speed compressors running at part load condition	Pearson (2019)
Too low suction pressure/ low evaporation temperature	incorrect control setting / designed for lower evaporation temperature than required	Pearson (2019), Cobo and Renilla (2015), Berglöf (2013)
	poor evaporator performance	Pearson (2019)
	blockage in compressor suction	Pearson (2019)
	insufficient charge	Berglöf (2013)
Too high discharge pressure	build-up of non-condensables	Pearson (2019)
	scale build-up on condenser tubes	Pearson (2019)
	higher condensing temperature due to ineffective control	Pearson (2019), Cobo and Renilla (2015)
	poor system design which requires a high head pressure to be maintained at all times	Pearson (2019)
	poor insulation of suction line	Prakash (2006)
Internal heat/gas leakage	direct leakage of high-pressure gas to the low-pressure side of the system due to faulty defrost or hot-gas bypass	Pearson (2019)
	direct internal leakage due to loss of liquid seal of expansion device	Pearson (2019)
	excessive wear and tear on compressors causing an increase of leakage from the discharge side back to suction	Pearson (2019), Cobo and Renilla (2015)
	non-optimal defrost timing	Pearson (2019)
Excessive auxiliary power consumption	over-sizing water drain line heaters	Pearson (2019)
	inefficient condenser fan control	Pearson (2019)
Negative superheat	liquid carry over to the compressor	Berglöf (2013)
	insufficient charge	Berglöf (2013), Prakash (2006)
High-temperature difference between secondary fluid and evaporation	insufficient charge	Berglöf (2013)
	inefficient evaporator control	Berglöf (2013)
Low discharge temperature	liquid carry over to the compressor	Berglöf (2013)
High chilled water pressure drop, reduced flow rate, low outlet temperature	severe fouling	Grimmelius et al. (1995), Cobo and Renilla (2015)
	mechanical damage	Grimmelius et al. (1995)
	clogging in chilled water circuit	Grimmelius et al. (1995)
High super heat	improper insulation	Cobo and Renilla (2015), Prakash (2006)
Heat loss and pressure drop	improper insulation	Cobo and Renilla (2015)
	malfuctioning of valves	Cobo and Renilla (2015)
High energy consumption	poor quality secondary fluid	Cobo and Renilla (2015)
	fixed speed rotating machines	Cobo and Renilla (2015)
	improper control logic for refrigeration system	Cobo and Renilla (2015)
	loss in frequency controller	Prakash (2006)
	insufficient charge	Grace et al. (2005)
Fluctuation in superheat and sub-cooling	hunting in expansion valve	Prakash (2006)
Almost zero sub-cooling	insufficient charge	Prakash (2006)
Low *COP*	insufficient charge	Goswami et al. (1997), Choi and Kim (2002), Cho et al. (2005), Tassou and Grace (2005)

*** Outside the research scope**

3

Verkade Plant Analysis

Recently Ntagkras (2022) has developed a digital twin (DT) of a chiller plant at the Verkade factory in the Netherlands. The DTs of the screw compressor, evaporative condenser, and evaporator were developed by Ntagkras (2022). In this chapter, the same DTs are reproduced and verified before developing the DTs for other installations described in the following chapters.

3.1. System details

The Verkade plant in Zaandam, the Netherlands uses BlueAstrum NH_3 Chiller 1000. The chiller is designed to supply chilled water with a temperature range of 6 to 12°C. Figure 3.1 refers to the piping & instrumentation diagram (PID) for the chiller used in the Verkade plant. The main components of the chiller are a screw compressor, an evaporator (plate heat exchanger), an evaporative condenser, and an expansion valve. The screw compressor compresses gaseous NH_3 to a higher pressure where it is in a superheated state. It goes via the evaporative condenser for heat rejection. After heat rejection, NH_3 is in a liquid state when it goes to the liquid receiver. From the liquid receiver, it goes through the expansion valve where the pressure is reduced. Then it enters the evaporator where the heat addition takes place as the water is cooled. At the outlet of the evaporator, NH_3 is again in the low-pressure superheated state which goes to the suction of the compressor. The water which is cooled by the evaporator is supplied to the plant for various applications. For the Verkade plant, the outlet water temperature of the chiller is the controlled variable.

3.2. Digital twin models

In order to analyze the Verkade plant, DT models of the major components of the chiller were developed. This section describes the equations used for developing the DTs, validation of DTs, and the results when applied to the actual plant data.

3.2.1. Screw compressor model

The DT models (for compressor power and capacity prediction) of the screw compressor are based on experimental data (saturated suction, discharge temperature, compressor power, and capacity) provided by GEA and an empirical equation similar to the equations (2.1 & 2.2) reported in the literature (Sahoo (2023)).
A similar equation[1] is used for the calculation of power consumed by the compressor with different

[1] **Note** - The temperatures for equations 2.1 and 2.2 are in °C.

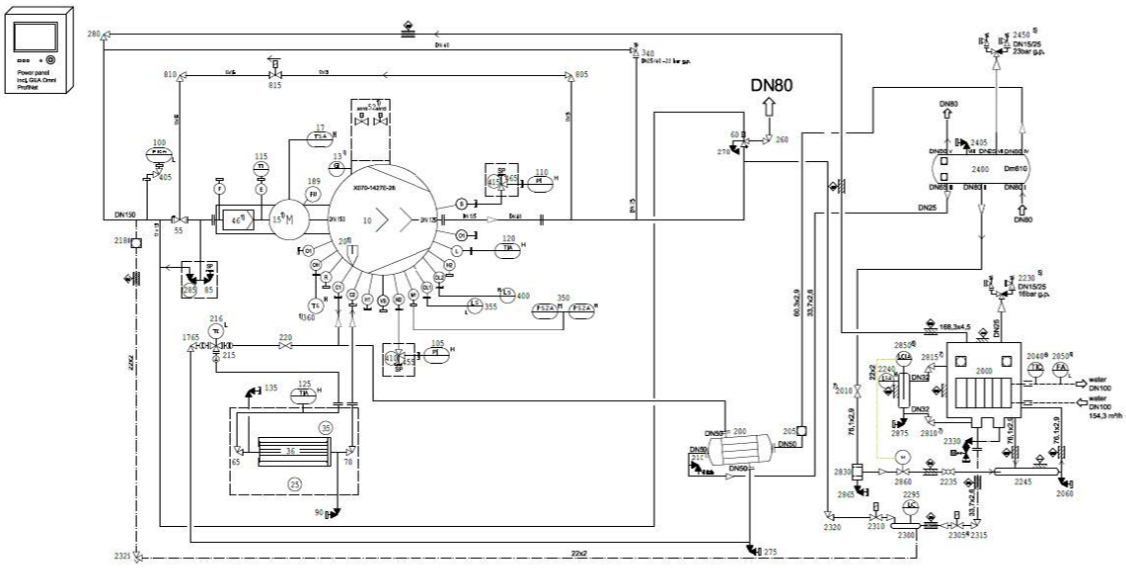

Figure 3.1: PID for BlueAstrum NH_3 Chiller 1000 (provided by GEA)

coefficients.
The coefficients of the equations were calculated using experimental data. The non-linear Generalized Reduced Gradient algorithm was used to calculate the coefficients. This algorithm calculates the coefficients in such a way that the compressor capacity and power predicted by the equations result in a minimum error with respect to the actual experimental value. The equations also consider the whole range of operating conditions they are, -5°C to 10°C for evaporating temperature and 15°C to 35°C for condensing temperature.
These equations were used to predict the cooling capacity and power consumption of the compressor. The validation was performed with experimental data. The root mean square (RMS) error for the equations were 2.32 kW and 0.1 kW respectively for capacity and power calculation.
Since the error percentages (0.3% and 0.1% respectively) for the compressor DTs were low enough, they were used to compare the actual cooling capacity and power consumed by the compressor running at the site. However, these models only predict the power and capacity of the compressor in full-speed conditions. So to calculate the power and capacity in the part load conditions speed, capacity, and power ratios of the compressor were used as inputs. Figure 3.3 shows the variation of cooling capacity and compressor power with the speed of the compressor. Ratios of power, capacity, and speed were calculated by dividing the individual values by the maximum values. These ratios were used to create two polynomial curves which give power ratio and capacity ratio as output when speed ratio is given as input. When these ratios for different compressor speeds are multiplied by the capacity and power output by equations 2.1 and 2.2, then the outputs are the capacities and power at the part load conditions.
The model with the correction for the part load conditions was used to predict the power consumption of the compressor. Figure 3.2 represents the comparison of power consumed by the compressor DT and the actual experimental values. It was observed that there was not much deviation in the actual and DT power consumption. Hence, it was concluded that the compressor was working as per the design and the compressor DT also worked fine.

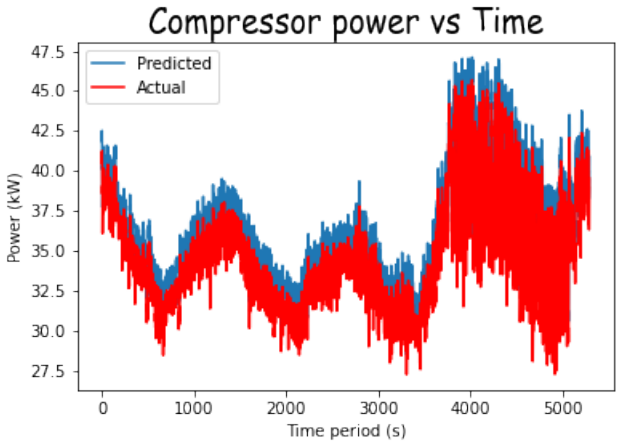

Figure 3.2: Comparison between actual and predicted compressor power consumption

Capacity	Cooling capacity	Shaft power	Evaporator Temperature	Condenser Temperature	Speed	EER
(%)	(kW)	(kW)	(°C)	(°C)	(RPM)	
100	1273	172	0	25	5200	7.4
95	1209	164	0	25	4950	7.39
90	1145	155	0	25	4700	7.39
85	1082	147	0	25	4450	7.38
80	1018	138	0	25	4200	7.37
75	954	130	0	25	3945	7.37
70	891	121	0	25	3690	7.37
65	827	112	0	25	3435	7.36
60	764	104	0	25	3180	7.36
55	700	95	0	25	2920	7.35
50	636	87	0	25	2660	7.33
45	573	79	0	25	2410	7.25
40	509	71	0	25	2160	7.14
35	445	63	0	25	1905	7.02
30	382	56	0	25	1650	6.87
25	318	49	0	25	1425	6.56
20	267	43	0	25	1245	6.24

Figure 3.3: Cooling capacity and power at part load conditions

3.2.2. Evaporative condenser model

The evaporative condenser model is based on the experimental data (saturated suction, saturated discharge temperature, compressor power, and capacity (% of full load)) provided by GEA, equations, and capacity factor (cf) table provided by the condenser manufacturer, and the outputs of compressor DT. The capacity factor table consists of capacity factors for each corresponding *WBT* and condensing temperature. So, if any of the two data are known then the third can be calculated. To predict the condensing temperature using the DT model, the condensing capacity was calculated using the compressor DT. Validation was done using the experimental data. The RMS error was 2.42 kW and the error percentage was 0.4%.
To calculate the condensing temperature first the nominal capacity was calculated using equation 2.3. The value for rated capacity was taken from table 3.1 while the value for capacity factor was taken from the table provided by the manufacturer, which is a function of *WBT* and condensing temperature at rated operating conditions. After the calculation of nominal capacity, the fan speed percentage was used as the input to equation 2.4 to calculate the capacity factor for all the data points of the plant using equations 2.4 to 2.7. The capacity factor and *WBT* were used to calculate the condensing temperature using the capacity factor table provided by the manufacturer.

Figure 3.4 represents the variation of condensing temperature with time. The first figure refers to the actual and predicted condensing temperature over the entire time period, while the second figure refers to the values over a particular time period. It was clear from the figure that most of the

Table 3.1: Rated condenser specifications

Model	CXVE 313-1012-15W
Type	Evaporative condenser
Condensation Temperature (°C)	36.69
WBT (°C)	27
Capacity (C_{rat} (kW))	1315
Fan power (kW)	2 * 5.26

predicted and actual values had on average 2°C temperature difference, but even 2°C deviation can lead to energy loss. Hence, it was concluded that the condenser was not working as per the design. The condenser DT was further investigated. The DT was used to calculate the condenser fan speed using the same set of equations used to calculate the condensing temperature with condensing temperature and *WBT* as inputs. Deviations were observed in the predicted and actual fan speeds, which confirmed that the condenser is underperforming and the DT model worked fine. Hence, the DT can be used for the other plants.

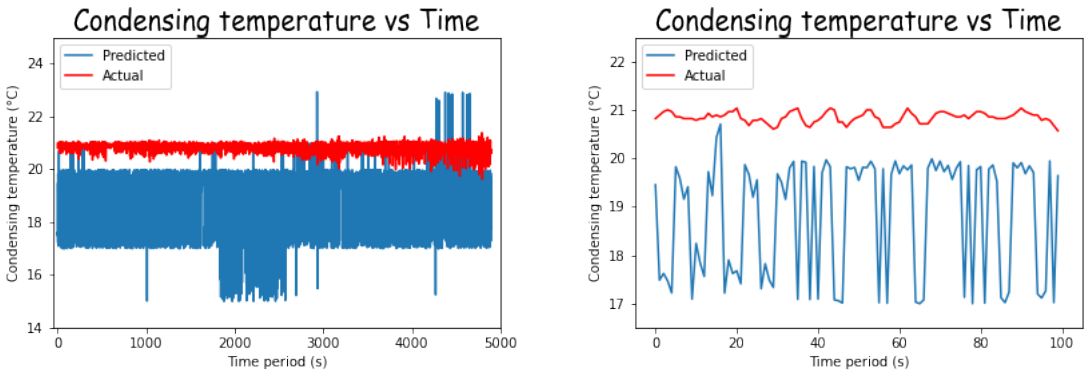

Figure 3.4: Comparison between actual and predicted condenser performance

3.2.3. Evaporator model

The evaporator model is based on the experimental data (cooling capacities and difference in outlet water temperature and saturated suction temperature) provided by GEA. These data were used to develop a 3^{rd} degree polynomial (refer to equation 3.1) which gives the difference in temperature as output when cooling capacity was given as input.

$$T_{wat,out} - T_{comp,suc} = -8.787 \cdot C_{evap}^3 + 1.66 \cdot C_{evap}^2 - 6.13 \cdot C_{evap} + 1.5676 \tag{3.1}$$

Figure 3.5 shows the evaporator model validation curve. The curve was plotted to check the accuracy of values predicted by the polynomial curve. The RMS error for the evaporator model was 0.05°C. Figure 3.6 represents the variation of temperature difference of the water outlet and the saturated suction temperature of the refrigerant. The first figure represents the actual and predicted temperature difference over the whole data set, while the second figure refers to the same temperature difference over a smaller time period. As the difference in predicted and the actual difference in temperature was more than the RMS error, that implies the evaporator was not working as per the design. In the second figure, it was observed that the control of the evaporator was not stable as the temperature was fluctuating too rapidly. The unstable behavior of the evaporator could be due to the control valve just before the evaporator. Hence, the liquid feed valve data was verified, as evident from the figure 3.7 the valve opening percentage of the liquid feed valve is unstable. So, it

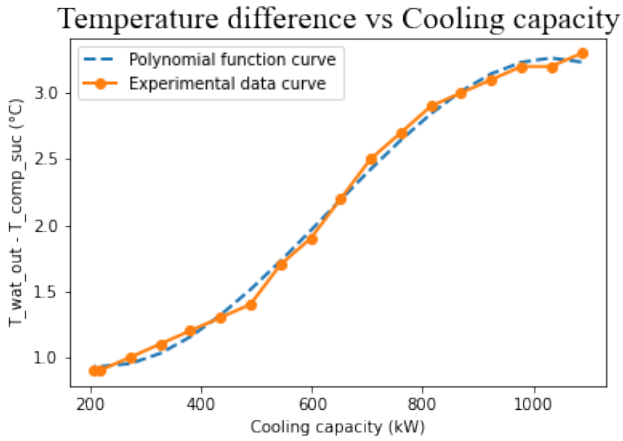

Figure 3.5: Evaporator model validation curve

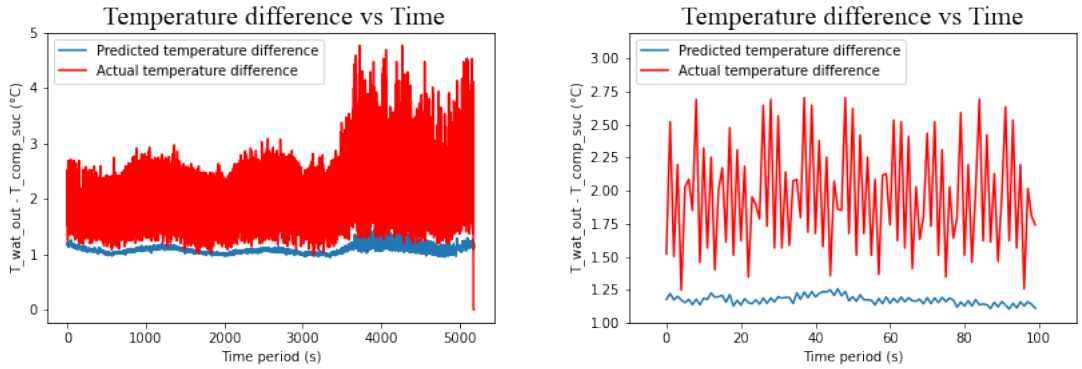

Figure 3.6: Comparison between actual and predicted evaporator performance

was concluded that the control of the evaporator in the plant needs modification.
However, the prediction by the evaporator DT was stable. Hence, a similar DT can be used for evaporator models.

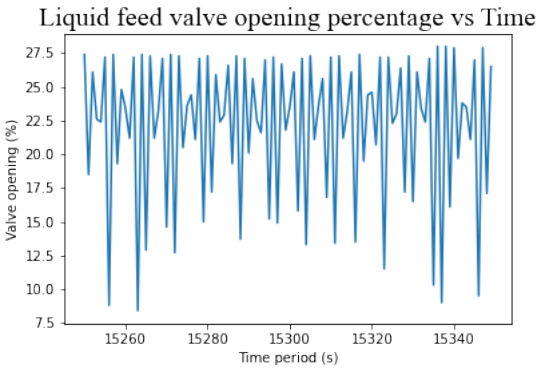

Figure 3.7: Instability in valve opening control

3.3. Optimal condensing temperature

From the literature research Sahoo (2023), figure 3.8 shows the variation of compressor power and condenser fan power with condensing temperature. From the figure, it is evident that as the con-

densing temperature is varied, the total power consumption changes and there exists one condensing temperature where the total power consumption is minimum. Hence, the optimum condensing temperature and the new power consumption were calculated for each data point.

The optimum condensing temperature set point was determined through an algorithm described

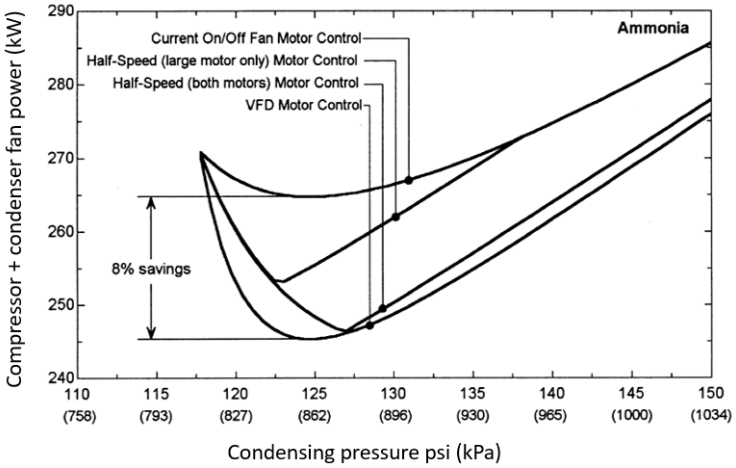

Figure 3.8: Variation of compressor power and condenser fan power with condensing temperature (Manske et al. (2001))

below to optimize the sum of the power consumption by the compressor and condenser fan.

1. Using the polynomial functions (equations 2.1 & 2.2), saturated discharge temperature, saturated suction temperature, and cooling capacity percentage (percentage of maximum cooling capacity at given operating conditions) calculate the total cooling capacity and total power consumption for the compressors.

2. Using the condenser equations (equations 2.4 to 2.7), dry bulb temperature, relative humidity, and condensing capacity (compressor power + cooling capacity) calculate the fan power and total power (fan power + compressor power consumption).

3. Assume the optimal condensing temperature to be 15°C. The suction temperature and the required cooling capacity still remain the same. Check if the capacity factor of the condenser (from the table provided by the condenser manufacturer) exists for the current operating conditions. If yes proceed with the following steps else check for higher condensing temperature till the capacity factor exists.

4. Calculate the new cooling capacity and new compressor power using the new condensing temperature.

5. Calculate the new EER (Energy efficiency ratio, new cooling capacity/new compressor power) in the new operating condition.

6. Calculate the required compressor power (required cooling capacity/new EER).

7. Calculate the condensing capacity (required cooling capacity + required compressor power).

8. Calculate the total power consumption as in step 2.

Figure 3.9 shows the condensing temperature before and after the optimization. Using this optimization technique a total of 7% energy can be saved annually.

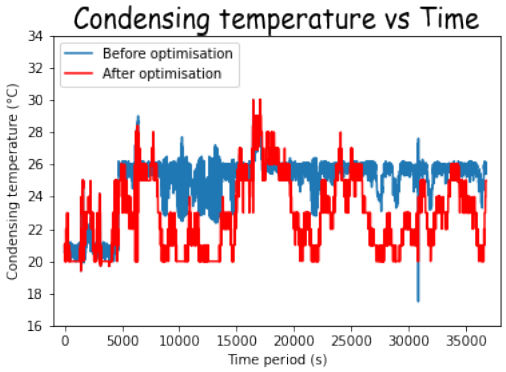

Figure 3.9: Condensing temperature before and after optimization

3.4. Conclusion

After verifying all the DT models it was concluded that the DT models are accurate within a 5% error margin and produce adequate results to analyze the equipment. Hence, the same model should be used for the analysis of further plants. The optimization of the plant produces energy savings of 7% annually. Around 32 MWh of electrical energy can be saved for the Verkade plant annually. This can save $ 13,000 and 11 tonnes of CO_2 per year. Reduction of CO_2 will mitigate the effects of global warming and help the governments meet the goals of the Paris Agreement.

4

LST Plant Analysis

The LST plant is located in Belzyce, Poland. The refrigeration system consists of mainly 2 screw compressors, 1 evaporative condenser, 3 freeze dryers and 2 air coolers (evaporators), and an economizer. The plant is designed to operate at -40°C throughout the year. Figure 4.1 represents the schematic of the LST plant. The operation of the LST plant is as follows. The screw compressors operate in parallel to compress NH_3, which then goes to an oil separator. The oil is removed from the refrigerant in the oil separator, then the refrigerant (with low oil content) goes to the evaporative condenser via the heat recovery unit. The heat from the system is released in the condenser and then the refrigerant goes to the liquid receiver. From the liquid receiver, there are two streams of refrigerant, the main flow is sub-cooled in the economizer and the other goes through the intermediate expansion valve before going through the other side of the economizer. The stream of refrigerant which passed through the intermediate expansion valve enters the compressor as a side stream. While the other stream of refrigerant which passed directly through the economizer passes through an expansion valve before entering the low-pressure liquid separator. The liquid refrigerant from the low-pressure separator is pumped into the evaporators (3 freeze dryer coolers and 2 air coolers). The refrigerant (two phases) from the outlets of the evaporator is received in the low-pressure separator. The vapor refrigerant from the low-pressure separator goes to the suction of the compressors.

Before analyzing the individual components, the behavior/validity of each type of data was analyzed to clean the data. It was observed that for some of the data points the compressor speeds were zero. That was due to shutdown or maintenance, the compressors were not running. Hence, those periods were removed from the analysis. Moreover, there were some data points for which the compressor speeds were below the minimum speed allowed for the compressor as per the design specification. That was due to the startup or shutdown of compressors. These points were not removed for two reasons, first to calculate the power consumption during the startup and second to understand the dynamic behavior of the compressors during startup.

From figures 4.2, it was observed that there was a large variation of suction and discharge temperature over an hour. The variation in temperature in the evaporator was due to the startup condition or multiple air coolers and freeze dryers were started simultaneously which led to a rapid increase in the cooling load. This increase in cooling load led to an increase in compressor speed which in turn created a spike in condensing temperature.

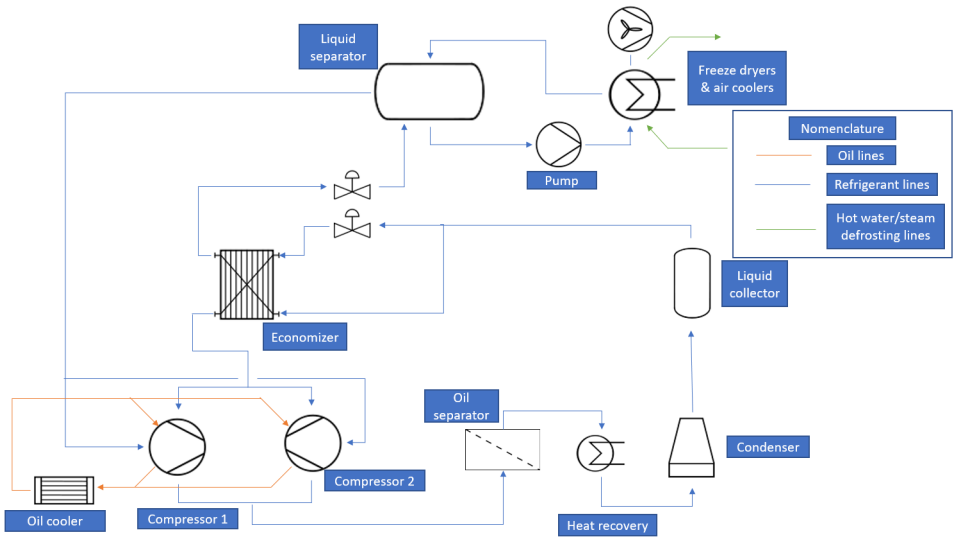

Figure 4.1: LST Plant schematic

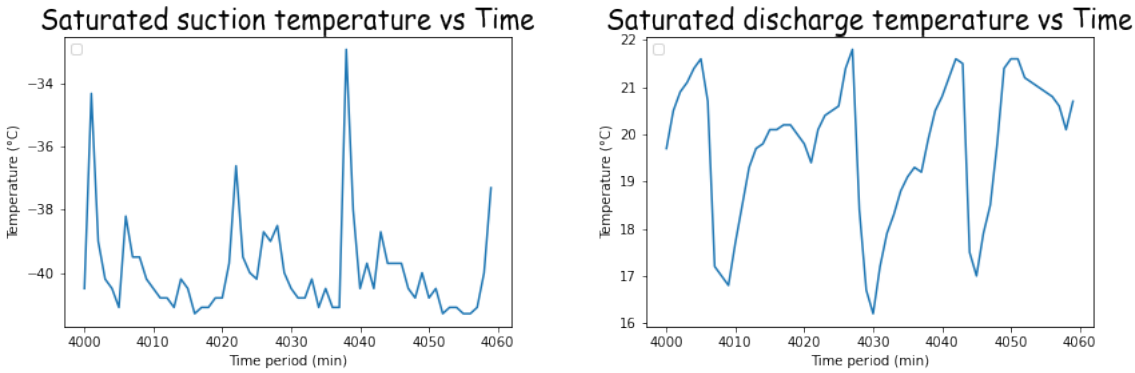

Figure 4.2: Suction and discharge temperature variation over time

4.1. Screw compressor model

The modeling of the screw compressor is similar to the compressor modeling of Verkade Plant as explained in section 3.2.1. The model was validated with the experimental data and the RMS error for the compressor power and cooling capacity was 11 kW and 13 kW respectively. The error percentages were 6.6% and 2.2% respectively.
From the actual plant data of the compressors, two inefficiencies were observed in the parallel operation, they were:

- both compressors were running in parallel even though the sum of their capacities was less than 100%.
- the compressors were running at different speeds.

The above-mentioned observations lead to a decrease in energy efficiency and hence, an increase in power consumption because the screw compressor's efficiency reduces drastically as its speed decreases (refer to figure 4.3). Hence, the following changes were required (based on literature findings) to optimize the parallel operation of the plant:

- when both the compressors were running at less than 100% of their capacities and the sum of their capacities was also less than 100%, only one compressor should be in operation.

- when the sum of their capacities was more than 100%, both compressors should be running at equal speeds.

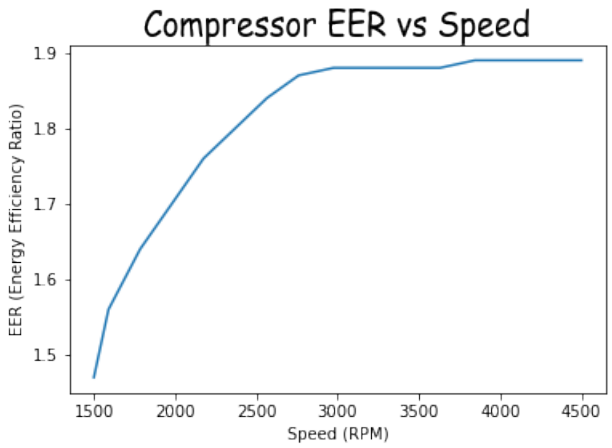

Figure 4.3: Energy efficiency ratio vs speed

4.1.1. Compressor optimization using the compressor speed as input

The above changes were used to optimize the parallel operation of the compressors. Before optimization, the compressors were running at different speeds and in some cases they were both running at less than 100% capacity. These operating conditions were leading to higher energy consumption. After optimization, when a single compressor could handle the load, only one compressor was in operation. In the other case when a single compressor could not handle the load, both compressors were operated at equal speeds.
The power consumption before and after the optimization for the same time period was analyzed. The power consumption was the same or the power consumption before the optimization was higher. The power consumption was the same implying that the compressors were already operating at optimized conditions or only one of the compressors was operating. While in other cases the optimized power is lower.
After the optimization, the total energy saved was 20,000 kWh for a year. This was 1.28% of the energy consumed by the operating compressors of the plant per annum.

4.1.2. Compressor optimization using the capacity percentage as input

The screw compressors used in the plant are of the variable volume type. That means the capacity of the compressor can be controlled by both sliding valve control and motor frequency/speed control. The effect of sliding valve control on the power consumption of the compressor was checked. Figure 4.4 shows that the slide valve position is 100% (maximum position) when the cooling load requirement is high. That means the compressor capacity at higher load requirements is controlled by the motor frequency/speed control. But when the compressor is starting or the cooling load requirements are low then the capacity of the compressor is controlled by the slide valve control and the speed is constant. This is because the compressor has a certain minimum design speed (1000 RPM) below which its efficiency drops drastically. As described in section 3.2.1, the compressor DT had the speed ratio as one of the inputs. But from the above explanation of compressor capacity control, it is clear that taking the speed ratio as an input will exclude the data points where the speed is constant and the control is done by the slide valve. Hence, it was decided to re-develop the DT model based on the capacity ratio instead of the speed ratio as an input. So to calculate the power and ca-

pacity in the part load conditions capacity percentage, capacity, and power ratios of the compressor were used as inputs. Ratios of power and cooling capacity were calculated by dividing the individual values by the maximum values. These ratios were used to create two polynomial curves which give the power ratio and capacity ratio as output when the capacity percentage is given as input. When these ratios for different compressor capacities are multiplied by the capacity and power output by equations 2.1 and 2.2, then the outputs are the capacities and power at the part load conditions.

All the analysis done previously with speed ratio as input was performed again with the capacity

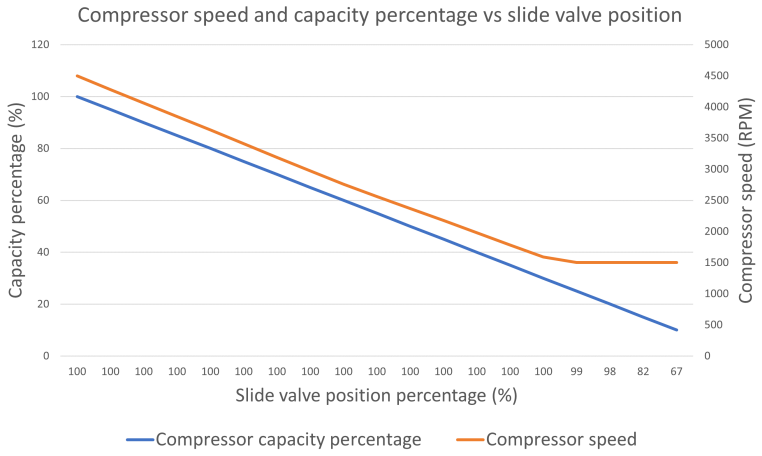

Figure 4.4: Slide position vs capacity percentage vs speed of the screw compressor

ratio as an input. Figure 4.5 shows the capacity percentages of the compressors before and after the optimization. While figure 4.6 refers to the power consumption before and after the optimization. Lastly, figure 4.7 refers to the power saved due to optimization. From the figures, it is evident that the observations are similar to the case when the speed ratio was used as an input. However, the total energy savings are increased.

After the optimization, the total energy saved was 25,000 kWh for a year. This was 1.55% of the

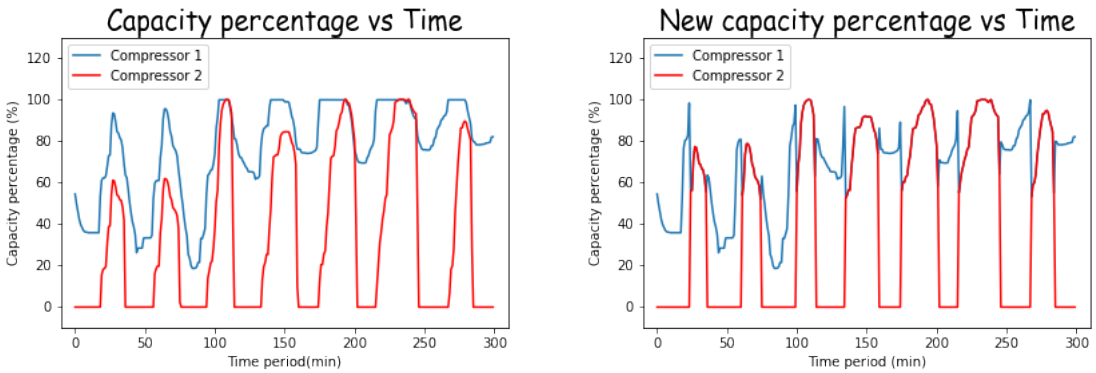

Figure 4.5: Capacity percentage for both compressors after capacity percentage was used as input

energy consumed by the operating compressors of the plant per annum.

4.1.3. Compressor power at startup

Further, it was observed (from figure 4.8) during the startup the power consumption by the compressor was higher than the power consumption predicted by the model. The reason is when the

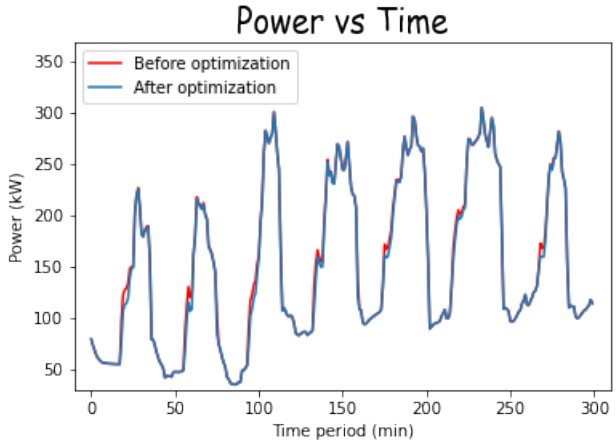

Figure 4.6: Comparison of power consumption for optimized and non-optimized compressors

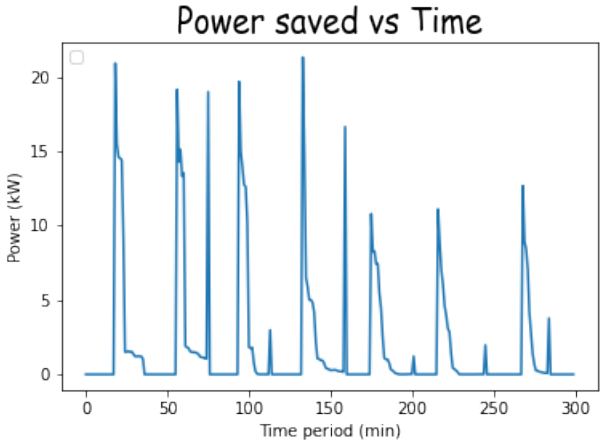

Figure 4.7: Power saved due to optimization

compressor starts the slide valve is in the most open position i.e. most of the discharge gas moves back to the suction, hence the power consumption is higher. So, to take this effect into account it was crucial to calculate the time required for the compressor to reach a steady state or lowest design speed. By using that time the model can be modified so that it predicts only the power consumption and capacity of the compressor in the steady state. However, it should be noted that the figure 4.8 x-axis doesn't represent the time required by a compressor to start, rather it is a cumulative time period of various compressor startups, which shows the power consumption is around 30 kW during all the compressor startups.

In comparison to the amount of energy consumed by the plant, the savings on energy consumption were quite low. Hence, a further investigation was done to understand the low power savings. The pie chart in figure 4.9 shows that 49% of the time only one of the compressors was running which does not lead to any energy savings. 50% of the time both the compressors were running and the sum of their capacities was above 100%, these cases lead to savings but very low. From these cases, the average saved energy was only 4.66 kWh. So, even if the number of cases was high, the savings were low. On the contrary, the average energy savings when both the compressors were running and the sum of their capacities were below 100% was 16.35 kWh. But this was only for 1% of the cases. Hence, the savings were again low.

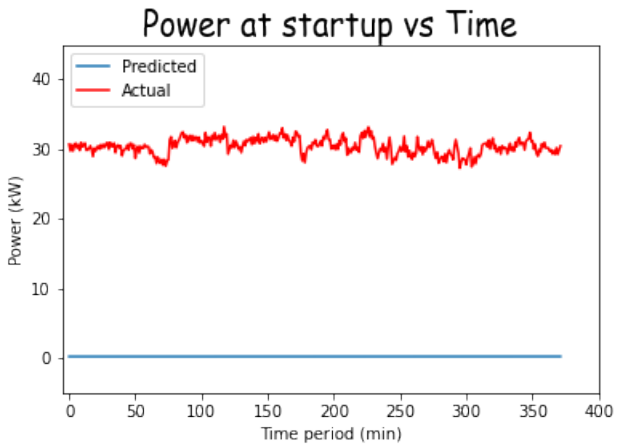

Figure 4.8: Comparison of predicted and actual power consumption during startup of the compressor (for 628 starts)

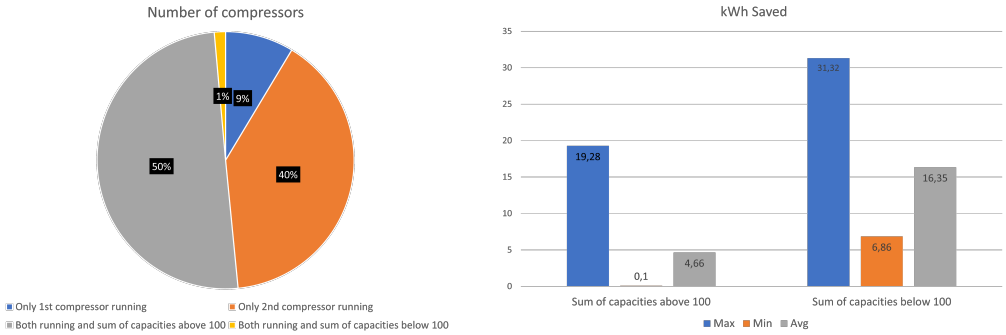

Figure 4.9: Pie chart representing the number of compressors running for 4 cases and bar chart representing the energy saved by 2 of those cases

4.1.4. Optimization of the number of compressors starts

Figure 4.9 shows that out of 49% of the cases when only one of the compressors is operating, only 9% of the time the first compressor is operating while 40% of the time the second compressor is operating. Further analysis showed that compressors were starting 16171 times in a year. This could result in severe mechanical wear in the second compressor. Hence, the total number of starts for both compressors was optimized. While the parallel operation optimization (optimization of load balancing) was done, the total number of starts was already down to 14418 from 16171 (refer to figure 4.10). This was the case when the second compressor was starting below 100% capacity. But to reduce the number of starts even further the second compressor was started below 100% and the increase in power consumption by the compressors was checked. Figure 4.10 shows that the power consumption was reduced initially due to the parallel operation optimization and so is the number of starts. With the decrease in the percentage below which the second compressor was starting, the number of starts decrease while the power consumption increases. Hence, there should be a balance between the number of starts and power consumption.

4.2. Evaporative condenser model

The model of the evaporative condenser was developed as described in section 3.2.2. But for the current plant, the fan speed of the condenser was not recorded. Since the condenser model uses fan speed as the input to predict the condensing temperature, it was decided to assume fan speed for certain temperature conditions. From figure 4.11 it was observed that there exists a dead zone

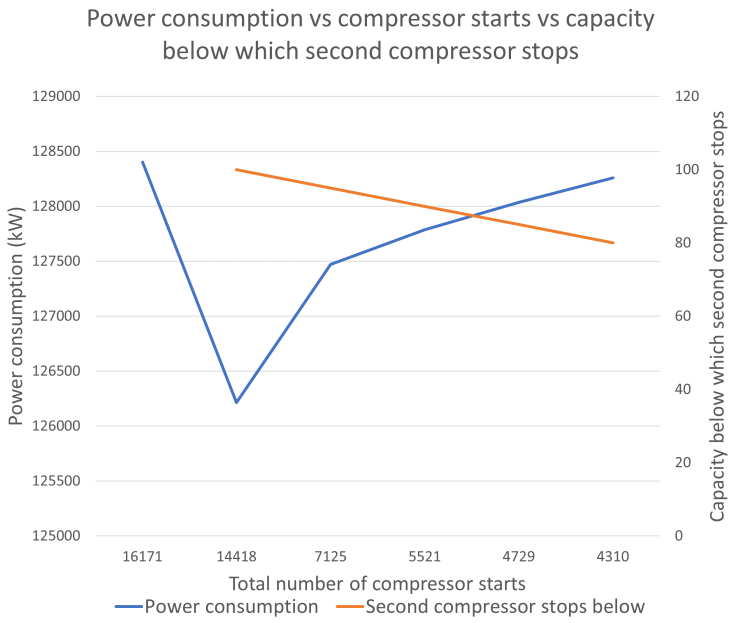

Figure 4.10: Variation of power consumption and the total number of compressor starts with the capacity below which the second compressor starts

for the condenser which was approximately 19-25°C. So, it was assumed that when the condensing temperature is fairly above this dead zone (around 28-30°C) and the *WBT* is high enough (above 10°C), the condenser fan is at full speed. Further analysis showed that these conditions were most prevalent in summer (months of July and August) and especially in the daytime. Hence, the condensing temperature was predicted based on these conditions.

The actual condensing temperature did not match the predicted condensing temperature, and the

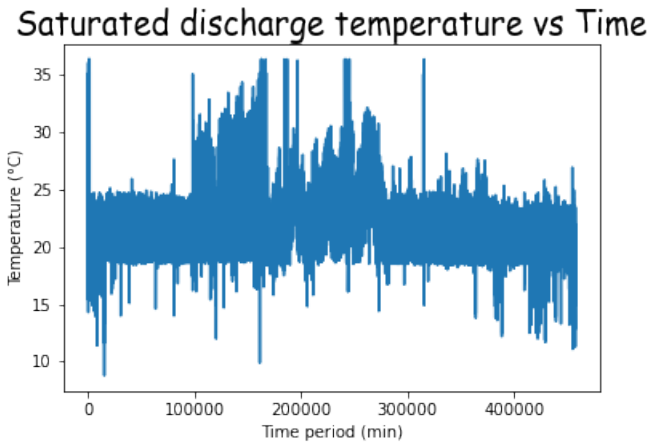

Figure 4.11: Temperature dead zone for condenser

deviation was almost 5°C for each data point. Since the model was already validated (at the Verkade installation) which uses the same evaporative condenser, the only possible error could be due to the sensor measuring the ambient temperature and humidity. These data could be verified from the nearby weather stations. Hence, the ambient temperature and humidity data for the plant location were collected. But the data from the nearby weather station was hourly and the data from the plant was per minute. Hence, first, the data from the plant was converted per hour and then it was

compared with the data from the nearby weather station. Figures 4.12 and 4.13 show the deviation of ambient temperature and *WBT* for the data set. From this, it was concluded that the data collected from the plant sensors were incorrect and the data from the weather station should be used for condensing temperature calculation.

Using the *DBT* and humidity data from the nearby weather station, the prediction for the condens-

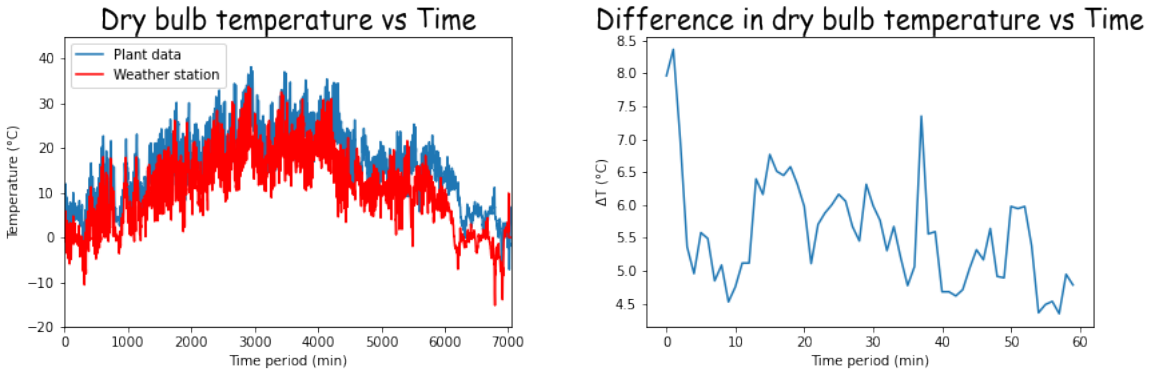

Figure 4.12: Deviation in DBT of plant data from the weather station

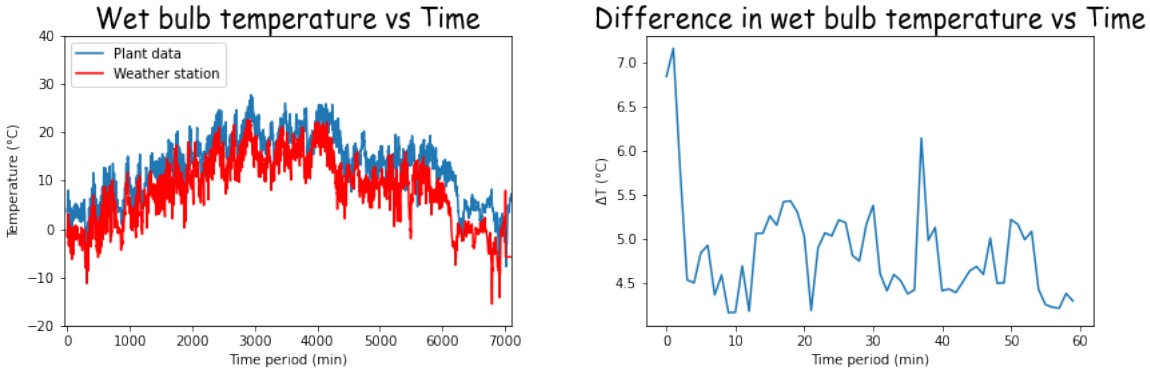

Figure 4.13: Deviation in WBT of plant data from the weather station

ing temperature was performed again. Figure 4.14 shows that the predicted condensing temperature is matching the actual condensing temperature within 1°C for most data points. Hence, this model can be used for the optimal condensing temperature calculation.

Calculating the optimal condensing temperature for a relatively huge data set takes a lot of computation time. So, the optimal condensing temperature was assumed to be 15°C for each data point and then the power consumption was calculated for each data point. For this calculation, the ambient temperature and humidity were used from the weather station data. Since, the data were hourly, to convert them to per-minute data it was assumed that the temperature and humidity remained constant over the hour.

4.2.1. Root cause analysis for condenser fan speed deviation

To calculate optimal condensing temperature, intermediate steps involved the calculation of fan power. To calculate fan power, the fan speed was calculated based on the condensing capacity predicted by the model. It was observed that the fan speed was above 100% for around 38% of the data points. Further investigation showed that the fan speed was going above 100% when the *WBT* was higher or in summer conditions. The fan speed was higher due to the high condensing capacity

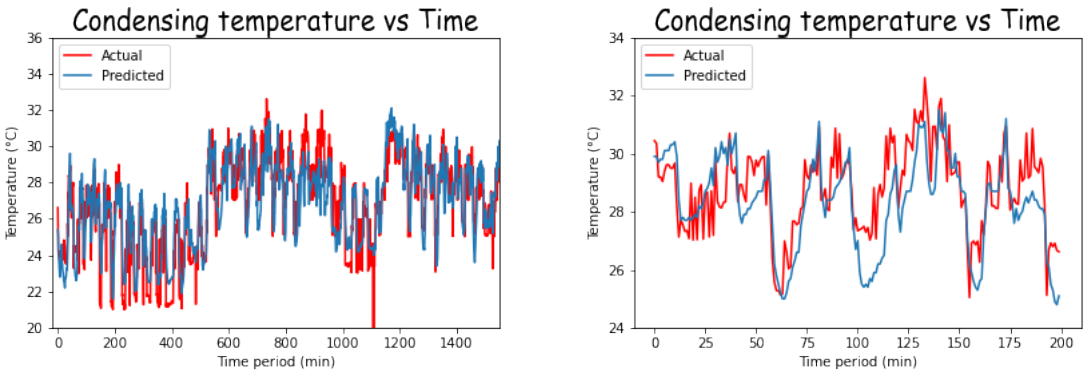

Figure 4.14: Condensing temperature actual vs predicted for the complete time period and a specific time period

predicted by the model. The reason for the high condensing capacity was investigated. Hence, as per the literature research and experts from GEA one of the possible reasons could be:

- oil cooling load not considered - the oil cooler used for the compressor was liquid cooled. Hence, the oil cooler cooling load should be subtracted from the condensing capacity.
- heat recovery not considered - there is a heat recovery system just before the condenser. In the data points where the heat recovery system was ON, the cooling load of the heat recovery system should be subtracted from the condensing capacity.
- defrosting not considered - the air coolers use hot gas defrosting and the freeze dryers use hot water defrosting. Hence, the data points where hot gas defrosting was used need to be taken into account.
- leakage in the condenser - there could be leakage of refrigerant from the discharge side to the suction side of the compressor.

All these possibilities were checked one by one and eliminated. First, the data points where defrosting was ON were checked and it was found that the defrosting didn't have any effect on the higher condensing capacity as there were many data points where there was no defrosting and still the fan speed was above 100%.
Second, to check the leakage of refrigerant from the discharge to the suction side, the expansion valve digital twin model was developed to check the cooling capacity. By comparing the cooling capacity calculated by the compressor and the expansion valve leakage could be detected. If the cooling capacity of the expansion valve DT is lower than the compressor DT then there should be a refrigerant leakage from the condenser. The expansion valve DT model is described in section 4.3. It was concluded that there was no leakage from the discharge to the suction side (refer to section 4.3).
Third, the cooling load of heat recovery was checked, and it was found that the cooling loads were insignificant to have such a large impact.
Finally, the oil cooling load was subtracted from the condensing capacity of the condenser and the fan speed was calculated again. To calculate the oil cooling load a DT model was developed for the oil cooler using the experimental values of cooling capacities of the oil cooler at various operating conditions. The experimental values include the cooling capacities at various saturated suction and discharge temperatures. Hence, equation 2.1 was used to calculate the oil cooler cooling capacities. However, the coefficients of the equation were different from the compressor cooling capacity equation. Equation 2.1 calculates the cooling capacity of the oil cooler at full load. So, to calculate the cooling capacities at part loads, the cooling capacities at various speeds of the compressors

were used to create a polynomial function. This function was used to calculate the oil cooling capacity when the speed of the compressor was given as an input. The RMS error of the DT model was 4.07 kW and this corresponds to an error percentage of 3.9%. Figure 4.15 shows that the fan speed percentage is still above 100% but the fan speed has been reduced in comparison to the fan speed when the oil cooling load was not subtracted. 29% of the data points were still above the 100% speed. Hence, it was concluded that the oil cooling load was not the only reason for the high condensing capacity.

As the four suspected possibilities of high condensing capacities were inconclusive, further inves-

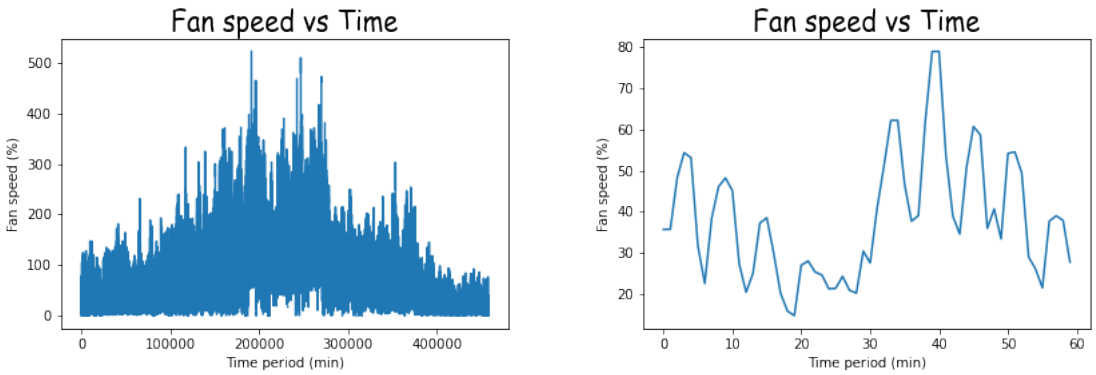

Figure 4.15: Fan speed for two different time periods after subtracting oil cooling load from the condensing capacity

tigation was done to understand the reason. From figure 4.16 it was observed that the temperature transmitters were in the individual compressor discharge lines and the pressure transmitter was placed in the combined line. To check the validity of data from the temperature transmitters, data from the pressure transmitter was used to calculate the cooling capacities and power consumption. However, it was observed that there was no major deviation in the results.

From further investigation, it was found that there were some time periods when all the coolers

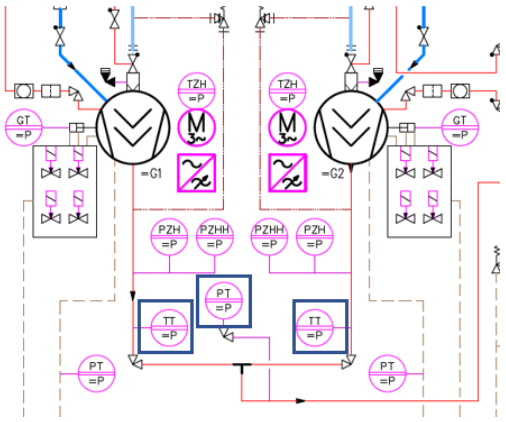

Figure 4.16: Part of piping & instrumentation diagram showing the transmitter locations

were stopped but the compressors and evaporator expansion valve were still operating. Figure 4.17 refers to those cumulative time periods for which the coolers were stopped but the compressors were operating. This is an indication that there could be a refrigerant thermal leakage from the condenser.

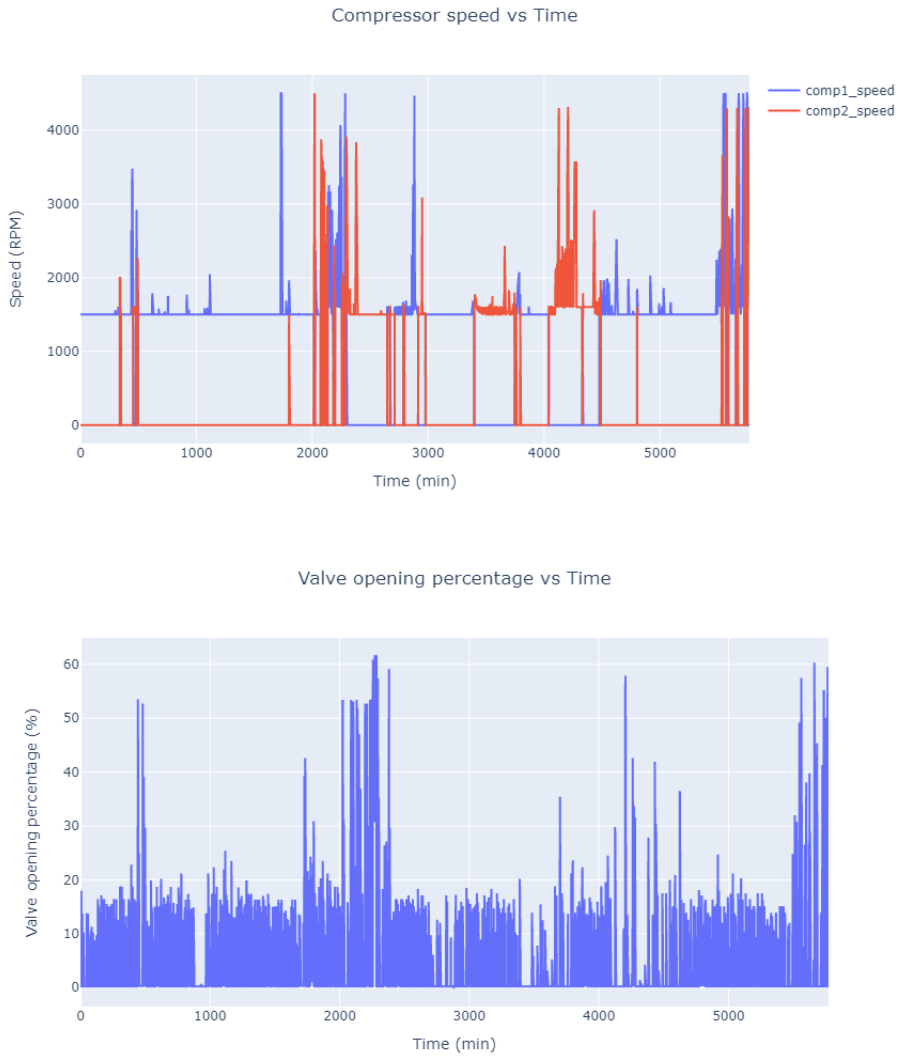

Figure 4.17: Figures representing the time period when compressors and expansion valves are operating while the evaporators are not operating

4.2.2. Optimal condensing temperature

As described in section 3.3, an optimal condensing temperature exists for each operating condition where the total power of the compressor and condenser fan is minimum. A different algorithm (than the one used for the Verkade plant) was used to calculate the optimal condensing temperature. The following algorithm describes the calculation procedure for optimal condensing temperature.

1. Using the polynomial functions (equations 2.1 & 2.2), saturated discharge temperature, saturated suction temperature, and cooling capacity percentage (percentage of maximum cooling capacity at given operating conditions) calculate the total cooling capacity and total power consumption for the compressors.

2. Using the condenser equations (equations 2.4 to 2.7), dry bulb temperature, relative humidity, and condensing capacity (compressor power + cooling capacity) calculate the fan power and total power (fan power + compressor power consumption).

3. Assume the optimal condensing temperature to be 15°C. The suction temperature and the

cooling capacity still remain the same. Check if the capacity factor of the condenser (from the table provided by the condenser manufacturer) exists for the current operating conditions. If yes proceed with the next steps else check for higher condensing temperature till the capacity factor exists.

4. Assume the cooling capacity percentage to be 30%. Calculate the total cooling capacity as per step 1.
5. Check if this cooling capacity is the same as the total cooling capacity calculated before optimization.
6. If yes then this is the cooling capacity percentage for both the compressors else increase the capacity percentage by 5% of the previous step.
7. Repeat the same steps till the cooling capacities match.
8. If the cooling capacities don't match at the highest capacity percentage, then increase the condensing temperature and repeat steps 4, 5, and 6.
9. Once the cooling capacities match for a particular capacity percentage, use that capacity percentage to calculate total power consumption as in step 2.

Figure 4.18 (left figure) shows the power consumption of the compressor and condenser fan using the optimal condensing temperature, while figure 4.18 (right figure) shows the difference in power consumption by using the optimal condensing temperature. It should however, be noted that it was assumed that the power consumption during the startup of the compressors was the same as before and the lowest condensing temperature of the condenser could be 15°C.
Total energy savings of 170,000 kWh was obtained which is 10.96% of the total energy consumption of the plant per annum.
Further studies were conducted to understand the complication of using a lower condensing temperature. It was found that by using a lower condensing temperature there could be oil carryover in the compressor. This is because the properties of the oil and refrigerant mixture change with temperature. There could be a possibility of the economizer not functioning due to the lowering of condensing temperature. Since the oil separator and expansion valve were suitable for 15°C, it was chosen to be the lowest possible condensing temperature.
The optimization was also performed using the algorithm described in section 3.3. Similar results

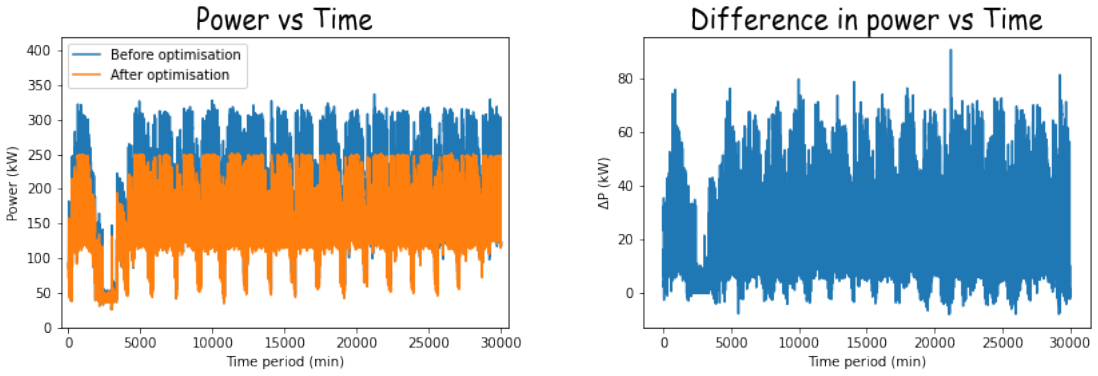

Figure 4.18: Total power (compressor + condenser fan) and difference in total power before and after optimization

were obtained, and total energy savings of 172,000 kWh was obtained which is 11.06% of the total energy consumption of the plant per annum.

4.3. Expansion valve model

For the expansion valve digital twin, experimental data (cooling capacities, saturated suction, and discharge temperature) were used to develop an empirical equation. Equation 2.1 was used to calculate the cooling capacity. However, the coefficients of the equation were different than the ones used for the compressor. The empirical equation used calculates the cooling capacities at 60% opening of the valve for different operating conditions as the experimental data used had cooling capacities at 60% valve opening percentage. So, to predict the cooling capacity at the actual opening percentage of the expansion valve, experimental data was used to develop a correlation curve between valve opening percentage and corresponding cooling capacities. This correlation was used to predict the cooling capacities at actual opening percentages. The RMS error of the DT model was 6.79 kW and this corresponds to an error percentage of 0.39%. Figure 4.19 shows that the predicted cooling capacity was unstable. So, the opening percentage of the expansion valve was verified and it was found that the valve opening percentage was unstable (refer figure 4.20) too. Hence, an average of cooling capacities were taken over 5 minutes to average out the variation. Figure 4.21 shows the cooling capacities predicted from the compressor model and expansion valve model. In general, the cooling capacities predicted from the expansion valve model were higher than the compressor model. If there was a leakage in the condenser then the cooling capacities predicted by the expansion valve model would be lower than the cooling capacities predicted by the compressor model. But that was not the case, hence it was inconclusive if there was refrigerant leakage from this particular study.

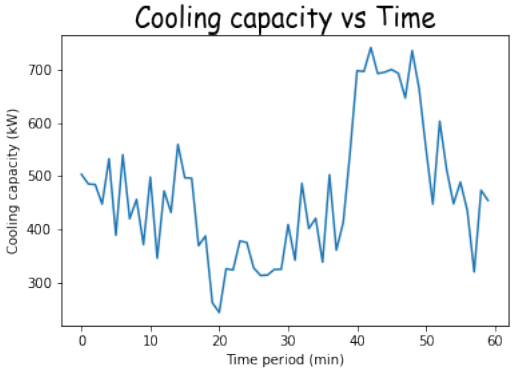

Figure 4.19: Instability in cooling capacity calculated using the expansion valve model

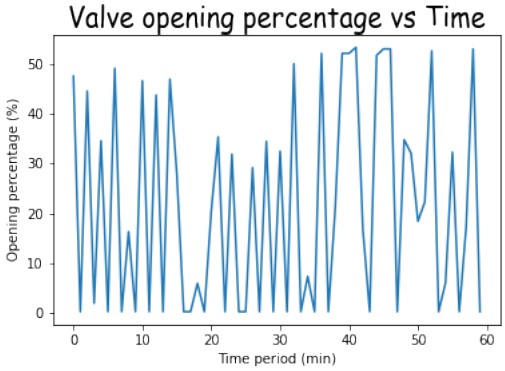

Figure 4.20: Instability in control of the expansion valve

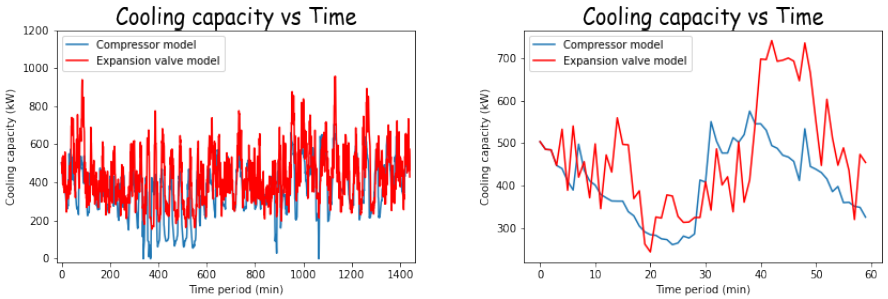

Figure 4.21: Cooling capacities for expansion valve and compressor model for two time periods

4.4. Evaporator model

To check the performance of the evaporators an evaporator model was developed. Since the evaporator start and stop times were the only data available, the cooling capacity calculated from the compressor model was used. To predict the cooling capacity first the individual evaporator cooling capacities were extracted by looking at the time periods when only one of the evaporators was running and all others were at a stop. Then the behavior of the individual evaporators was averaged out over the whole time period. Figure 4.22 shows the cooling capacities of freeze dryers and air coolers over a certain time period. The behavior of some freeze dryers (freeze dryers 1, 3 & 5) and air coolers was as expected. First, when the freeze dryers were started the cooling capacities were high due to dynamic effects and then the capacity comes down to a steady value over time. However, the other freeze dryers' (freeze dryers 2, 4 & 6) cooling capacities were increasing for a certain time period before going down. To identify the root cause, the cooling capacity of a single freeze dryer was checked (refer to figure 4.23). It was observed that, for the control of the LST plant two separate control systems are used one for the freezing process and the other for the steam defrosting process and there is no link between these control systems. Hence, the opening and closing of the valve timing may not be synchronized correctly, which could lead to the observed behavior. The second reason could be the type of food frozen in the freeze dryer. Different types of cooling capacity behaviors were observed in the freeze dryers which could be due to the type of food frozen.
A lot of energy is wasted because of the increase in cooling capacity at the start of the freezers. This can lead to some energy savings if corrected. However, it is difficult to quantify how much energy can be saved from this.
Figure 4.22 shows that the air coolers are continuously operating at 100 kW capacity but they are designed for a much lower capacity. That implies the control of the room temperature is not as per the design (refer to figure 4.24) leading to higher capacities. Further investigation implied that the cold store associated with cooler 7 is switched off when it is not required, while cooler 8 is always in operation, hence, the difference in temperature. The starting and stopping of coolers are energy-intensive processes because the room temperature goes up when coolers are not working, hence leading to higher energy consumption during startup. In conclusion, the temperature of the room can be maintained in an efficient manner to lower the cooling capacities and save energy.

4.5. Conclusion

After the analysis of the LST plant, the following is the conclusion:

- Screw compressors operating in the LST plant are not optimized for load sharing, hence, consuming higher energy. The compressors have unequal operating hours which leads to more mechanical wear in one of the compressors. This also leads to a higher maintenance frequency of one of the compressors. Due to inefficient control of screw compressors the num-

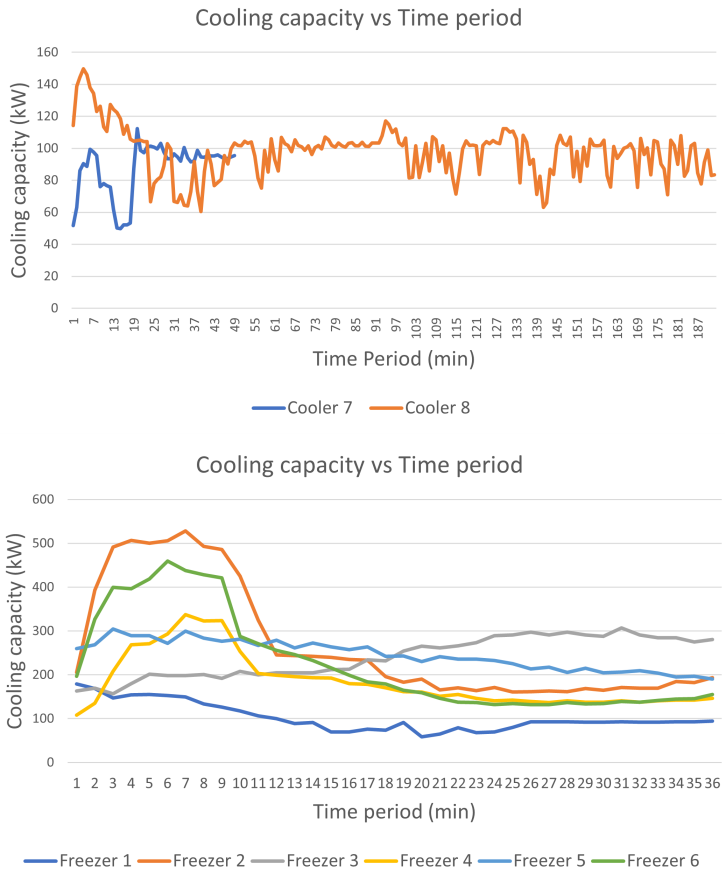

Figure 4.22: Cooling capacities for freezers and coolers

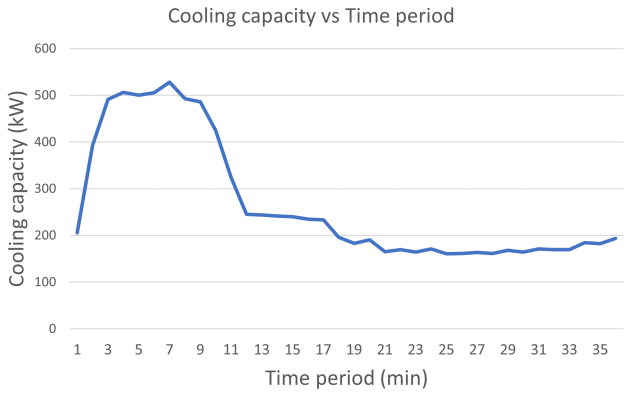

Figure 4.23: Cooling capacity for a freezer over a certain time period

ber of starts and stops is significantly high. Hence, the load sharing should be optimized in such a way that there should be a balance between the power consumption by the compressors and the total number of starts and stops.

- The evaporative condenser most probably has a refrigerant leakage or thermal leakage as the compressors and expansion valve are operating when all the freezer dryers and air coolers are not operating. Hence, the predicted fan speed is beyond 100% for many cases. The possibility of refrigerant leakage from the condenser should be checked.

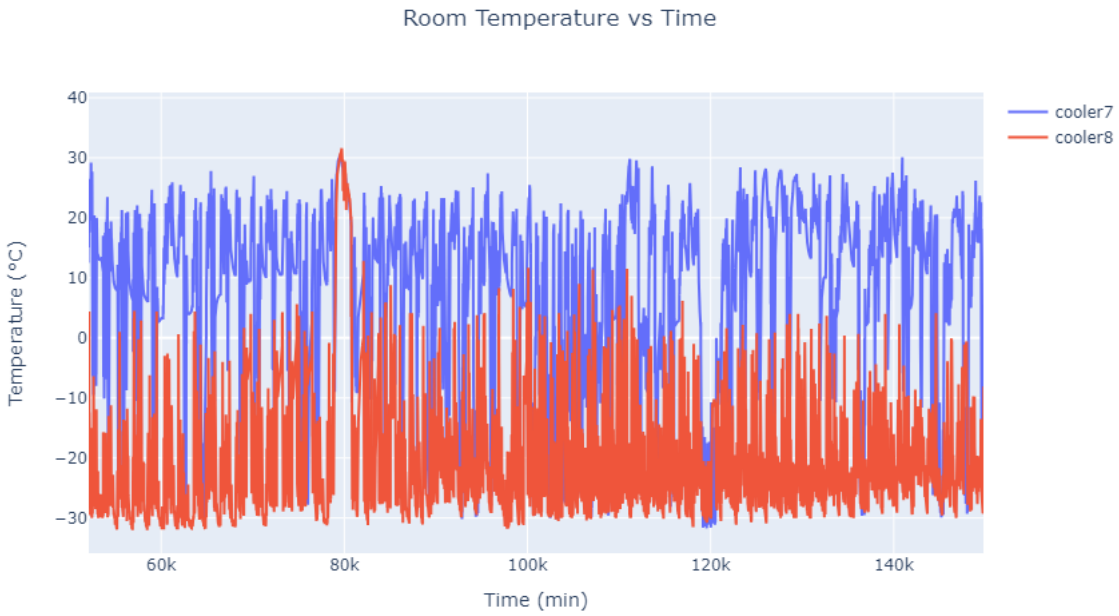

Figure 4.24: Variation of room temperature over time

- The expansion valve opening control is highly unstable. So, the control of the expansion valve opening should be rectified to make it more stable.
- The start-up phase of the freeze dryer results in significant energy loss due to increased cooling capacity. Design changes can lead to substantial energy savings in the freeze dryer. Additionally, the cooling capacities and energy consumption of the rooms cooled by the air coolers are higher due to inadequate room temperature maintenance. Proper room temperature control is necessary to address this issue.
- After all the faults are corrected the energy savings strategies should be applied. An energy savings of 1.55% can be obtained with the optimization of the parallel operation of screw compressors. While an energy savings of 11.06% can be obtained with the optimization of condensing temperature set point. With the correction of the evaporator design more energy can be saved but it is difficult to quantify. A total of approximately 200 MWh of energy can be saved per annum with these optimizations. This can save LST plant $ 81,000 per year on electricity costs, which in turn can save 70 tonnes of CO_2 from being released into the atmosphere. A decrease of CO_2 level in the atmosphere will help mitigate global warming and aligns with the goals of the Paris Agreement.

5

GIST Plant Analysis

The GIST plant is located in Crewe, UK. The refrigeration system consists of mainly 2 Ammonia chillers, 2 hybrid fluid coolers, and 11 air coolers (refer to figure 5.1). A hybrid fluid cooler is an adiabatic cooler that has both dry and wet modes of operation. At lower load requirements dry mode is used while at higher load requirements wet mode is used. In the dry mode, the cooling is achieved only through the cooler fan while in wet mode the cooling is achieved via both the cooler fan and water being sprinkled.
Two identical chillers are operated in parallel. The chiller outlet has two circuits, cold and hot glycol circuits. The cold glycol outlet temperatures from these chillers are controlled and kept constant. The cold glycol from the chillers is pumped through the air coolers. The glycol from the air coolers then returns to the cold glycol inlet of the chillers. The hot glycol outlet temperatures from the chillers are also kept constant. The hot glycol from the chillers is pumped through the hybrid fluid coolers. The glycol from the coolers then returns to the hot glycol inlet of the chillers.
The chiller has a screw compressor, an evaporator (plate-type heat exchanger), and a condenser (plate-type heat exchanger). The ammonia refrigerant (vapor) is compressed by the compressor to a higher pressure which then goes through the condenser. In the condenser, the refrigerant (two-phase) exchanges heat with the hot glycol circuit. The refrigerant (liquid) then goes through the expansion valve where the pressure is reduced. The low-pressure refrigerant (two-phase) passes through the evaporator where it exchanges heat with the cold glycol circuit. Again the vapor refrigerant passes through the compressor.
Before analyzing the plant, first, the data was cleaned. There were many data points for which the speed of both compressors was zero which implies that there was a shutdown or maintenance. These data points were removed. There were three data sets too for three different sets of time periods. So, the data was synchronized for a common time period.

5.1. Screw compressor model

The modeling of the screw compressor is similar to the compressor modeling of Verkade Plant as explained in section 3.2.1. The model was validated with the experimental data and the RMS error for the compressor power and capacity was 3.3 kW and 66.4 kW respectively. The error percentages were 1.85% and 3.43% respectively.
Since the error for the capacity model was high, two separate models were developed, one for condensing temperature higher than or equal to 30°C and the other one for condensing temperature lower than 30°C. The model was validated again and the RMS error for these models was 20.98 kW and 15.15 kW. The error percentages were 4.9% and 0.85% respectively.

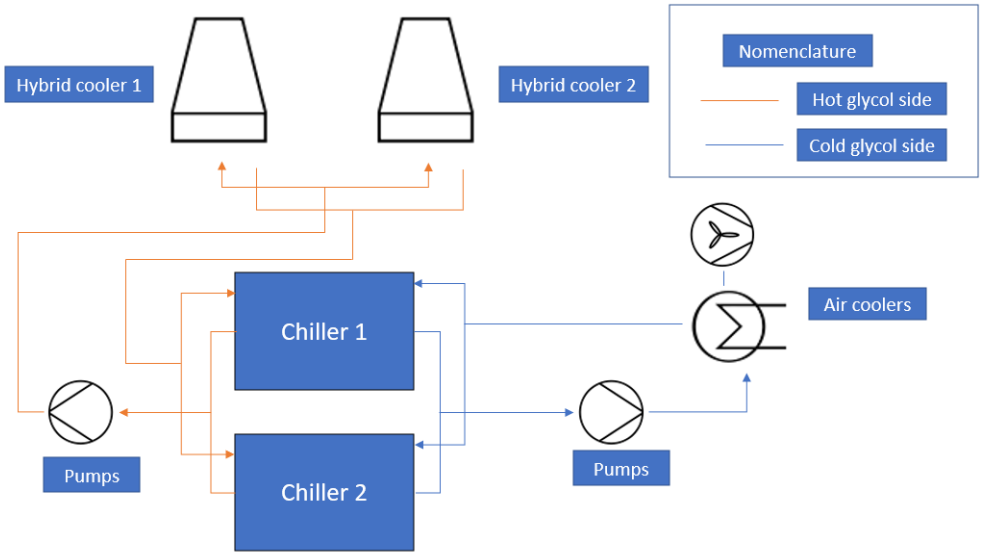

Figure 5.1: GIST Plant schematic

Figure 5.2 compares the predicted and actual compressor power consumption. The actual and predicted power consumption was quite similar. The average deviation and percentage deviation in performance were 9.22 kW and 9.17%. One of the reasons for the deviation was that the power consumption recorded at the plant did not consider the efficiency of the electric motor. Hence, the actual power consumption should be lower than the recorded values. The same figure also shows that there are some data points for which the power consumption is close to zero. From further analysis, it was concluded that those were the cases where the compressors were starting.

As described in section 4.1, the parallel optimization of screw compressors is possible to balance

Figure 5.2: comparison of actual and predicted compressor power over a time period

the loads in such a way that the compressors run at a higher energy efficiency ratio (refer to figure 4.3). The same is possible for the chillers as well. However, it should be noted that in the LST plant, the compressors are operating in parallel, but in the GIST plant, the chillers are operating in parallel. Hence, the chiller parallel operation was optimized as a whole instead of compressors. The chillers were optimized using the same algorithm as used for the LST plant. After optimization, energy savings of 2.42% was achieved. This can save 22,000 kWh of energy for the plant annually.
The plant records the number of hours each chiller has run. This data was used to create an algorithm such that the chillers run an equal amount of time. As per the algorithm, when both the chillers are running and one chiller has to be stopped because of lower load requirements, the chiller with higher operating hours is stopped.

5.2. Evaporator model

The evaporator (plate heat exchanger) model of the chiller was developed using a similar model as described in section 3.2.3. A similar 3^{rd} degree polynomial equation was used as in equation 3.1. However, the coefficients of the equation were calculated based on the experimental data for the evaporator model used in the GIST plant. The RMS error for the model was 0.01°C. It should be noted here that all the calculations were performed assuming a constant glycol mass flow rate.
Figure 5.3 compares the actual and predicted difference in temperature between the glycol outlet temperature and compressor suction temperature. The average difference in the actual and predicted values was 0.47°C for the chiller 1 evaporator, while it was 0.82°C for the chiller 2 evaporator. However, the deviation in temperature could be due to the variation in glycol mass flow rate in the actual plant because a constant glycol mass flow rate was assumed for the calculation of the difference in temperature. Hence, a mass correction was introduced to correct the cooling capacities calculated using the compressor model in accordance with the actual mass flow rate. For mass correction, the plate heat exchanger model was studied to find out the relation between the cooling capacity and glycol mass flow rate. It was observed that the cooling capacity of the evaporator varied in proportion to the glycol mass flow rate. The design (constant) glycol mass flow rate is known. Hence, first, the cooling capacity was calculated with the constant mass flow rate using equation 3.1. Then the cooling capacity was corrected in proportion to the actual glycol mass flow rate. After the correction was applied, the deviation in temperature difference still remained. This concludes that the evaporators for both chillers were not performing as per the design, especially the chiller 2 evaporator has a significant deviation. Hence, further investigation was performed to understand the root cause of the deviation.

As there was a deviation in performance in the evaporator model, further investigation was performed by calculating the cooling capacity from other available parameters of the GIST plant. For each chiller, the cold glycol flow rate, cold glycol inlet, and outlet temperature were available. The properties of the glycol (30% Glycol) used were also available. So, the specific heat capacity at the average of the inlet and outlet temperature of the cold glycol was calculated. Using the equation 5.1, the cooling capacity of the evaporator was calculated. The total cooling capacity was obtained by adding the cooling capacity of each evaporator.
The measured cooling capacity was compared with the cooling capacity calculated from the compressor model in section 5.1. Figure 5.4 refers to the comparison of the cooling capacities between the measured cooling capacity and the cooling capacity predicted by the compressor model over a certain time period. From the top figure 5.4 it was concluded that the evaporator was not performing as per the design as the predicted cooling capacity of the compressor model was higher than the energy model most of the time. From close observation (refer to bottom figure 5.4) over a short period of time it was concluded that the measured cooling capacity remained low at the start of the cooling process, then it gradually increased and finally, the cooling capacity was equal when the

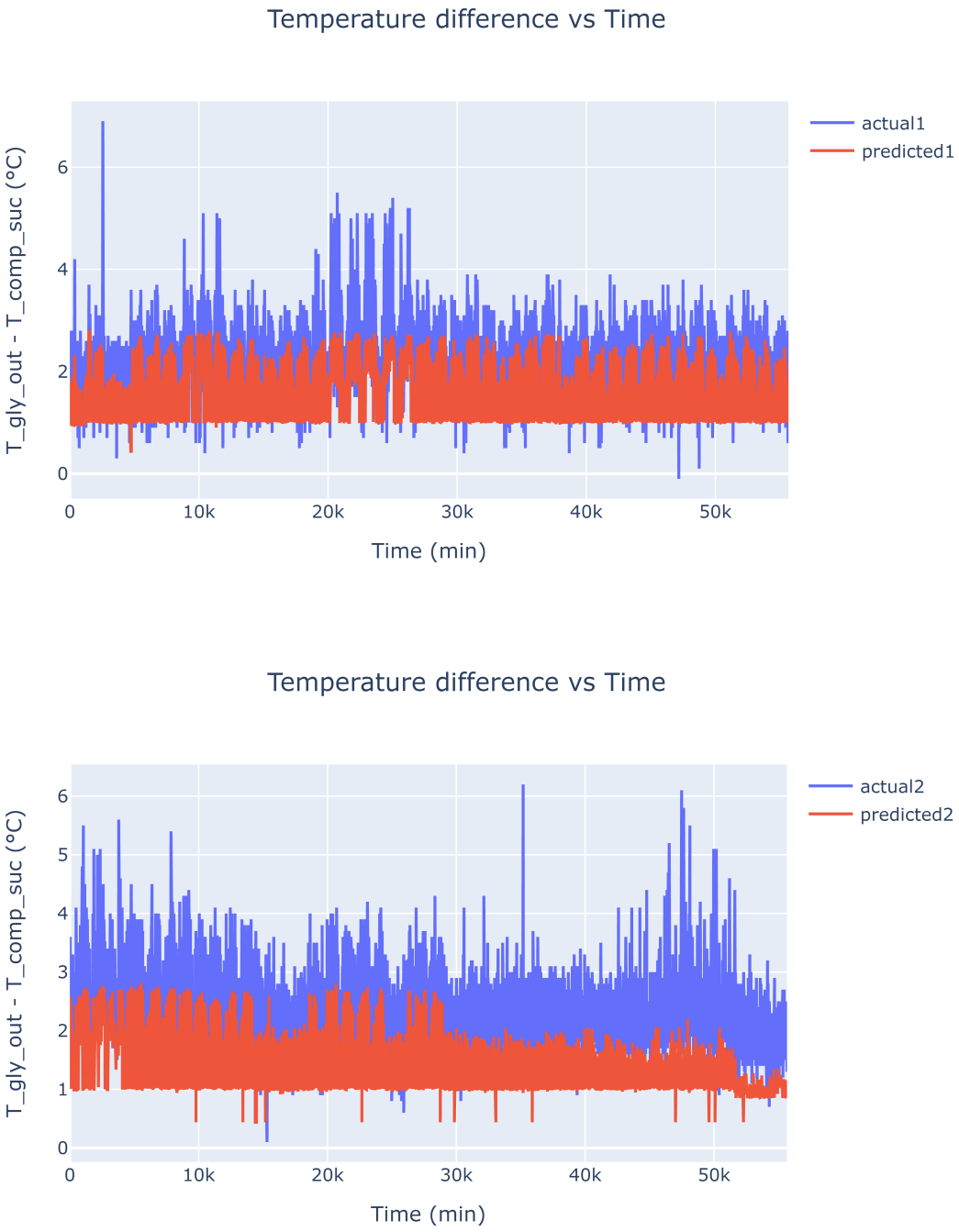

Figure 5.3: comparison of the actual and predicted temperature difference between the glycol outlet temperature and compressor suction temperature over a time period

defrosting was started. This pattern continues throughout the process.

$$C_{evap} = \dot{m} \cdot cp \cdot (T_{gly,in} - T_{gly,out}) \tag{5.1}$$

As per the Food & Drink Federation, UK (Food & Drink Federation et al. (2007)) and United Nations Environment Programme, US (United Nations (2018)), 1°C difference in temperature can lead to a 2-

Figure 5.4: comparison of the cooling capacity of evaporator for compressor model and the measured cooling capacity over a time period

5% difference in energy consumption. From the evaporator analysis, an average difference of 1.29°C was calculated. Hence, with necessary design changes, 3-5% energy savings can be achieved.

5.3. Condenser model

The condenser used in the chiller is a plate heat exchanger type. Hence, the model of the condenser was developed using a similar model as described in section 3.2.3. A similar 3^{rd} degree polynomial equation was used as in equation 3.1. However, the coefficients of the equation were calculated based on the experimental data for the condenser model used in the GIST plant. The RMS error for the model was 0.1°C. Similar to the evaporator, the condenser calculations were also performed assuming a constant glycol mass flow rate.

Figure 5.5 compares the actual and predicted difference in temperature between the glycol inlet temperature and compressor discharge temperature. The average difference in the actual and predicted values was 0.74°C for the chiller 1 condenser, while it was 0.41°C for the chiller 2 condenser. For the chiller 2 condenser, the temperature difference was negative for many data points. Further analysis showed that there were numerous data points where the second chiller was started only for a few seconds and then stopped. Hence, for these points even though the speed of the compressor was high enough, the compressor did not run for enough time for the temperature difference to become positive. It was concluded that the control of the chiller could be improved to avoid these short startups of compressors.

Moreover, the deviation in performance could be due to the assumption of constant glycol mass flow rate, when calculating the condensing capacity. A similar correction factor could be applied to the condensing capacity based on the glycol mass flow rate. But for the condenser side, there was no flow measurement in the GIST plant. Hence, a comparison with the measured data could not be performed.

Figure 5.6 shows the comparison of actual and predicted temperature differences between glycol inlet temperature and compressor discharge temperature after filtering out the negative values. Negative values were filtered out to get a more accurate deviation in performance when the chiller was not in startup condition.

After condenser performance analysis, it was concluded that there was an average temperature difference of 1.15°C. Hence, energy savings of 3-5% can be achieved with necessary design changes (considering the guidelines Food & Drink Federation et al. (2007) and United Nations (2018)).

5.4. Hybrid cooler model

The hybrid cooler has two modes of operation dry and wet, hence, the model was divided into two models based on the modes of operation. First, the model was developed using empirical equations but the deviation in cooling capacity prediction was large. So, machine learning techniques were also used to develop the model. The following subsections describe the cooler models using empirical equations and machine learning techniques.

5.4.1. Cooler model using empirical equations

Dry-mode model

First, the model for the cooler in dry mode was developed using an empirical equation. Cooling capacity, ambient temperature, glycol inlet temperature, glycol outlet temperature, glycol mass flow rate (constant), cooler fan speed, and cooler fan energy consumption were the supplier's data, that was used to develop the empirical equation. Correlation analysis of these data shows that the cooling capacity depends linearly on the difference in temperature between glycol inlet temperature and ambient temperature, while it depends non-linearly on the cooler fan speed. Hence, the empirical equation developed based on the correlation analysis is as shown in the equation 5.2.

$$C_{cond} = k_1 \cdot (T_{gly,in} - DBT) \cdot (FS\%)^{n_1} + k_2 \tag{5.2}$$

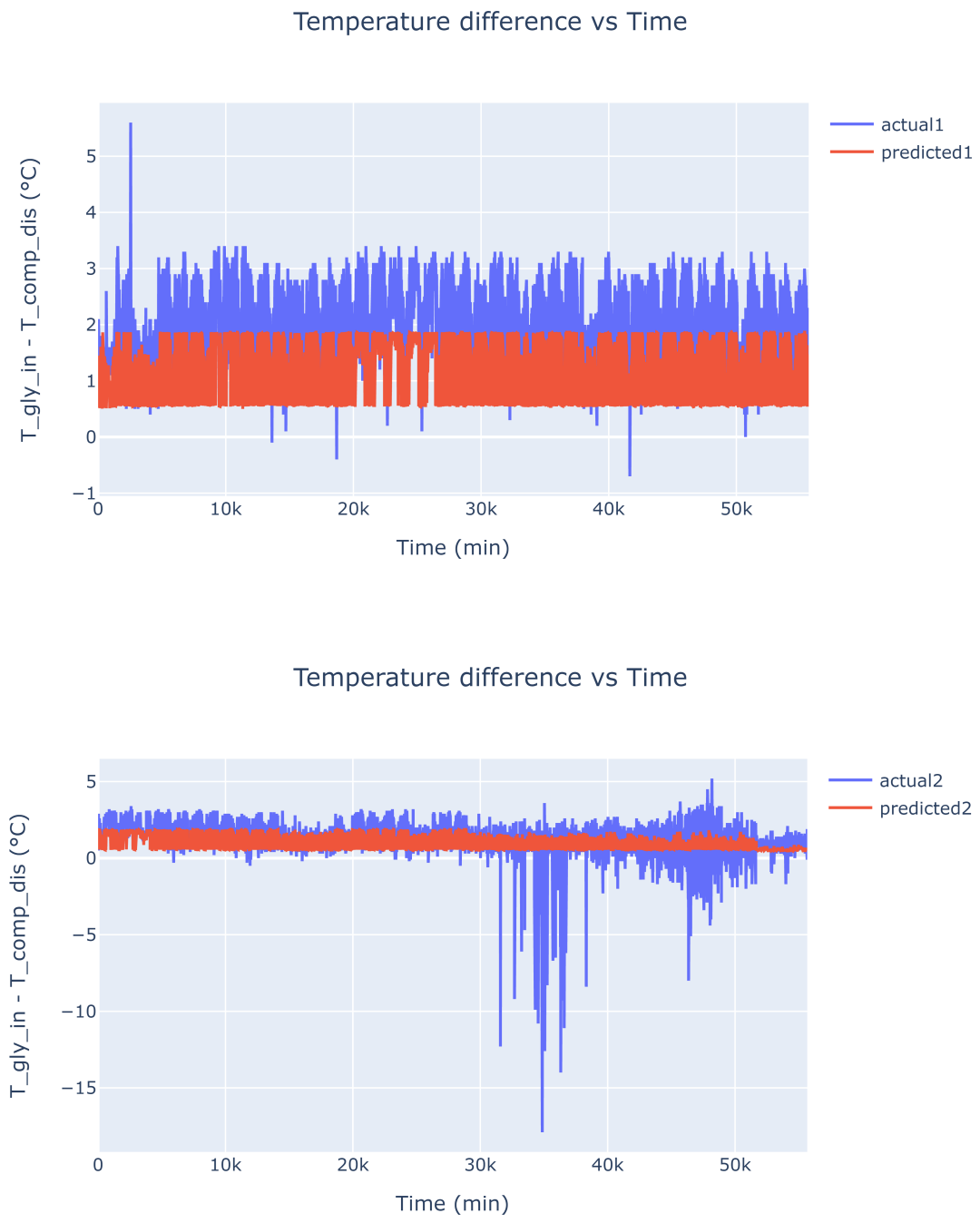

Figure 5.5: comparison of the actual and predicted temperature difference between the glycol inlet temperature and compressor discharge temperature over a time period

Supplier data were used to calculate the coefficients k_1, k_2, and n_1. The coefficients were calculated as 105.68, -103.49, and 0.84. Validation was performed for the equation to check the accuracy of predicting the cooling capacity. The average percentage deviation was 5.17% while the maximum percentage deviation was more than 50%. Hence, the equation was not suitable for the given Supplier data. To increase the accuracy of the model the data was divided into high-speed (greater than 20% of the maximum speed) and low-speed data (lower than 20% of the maximum speed) and then

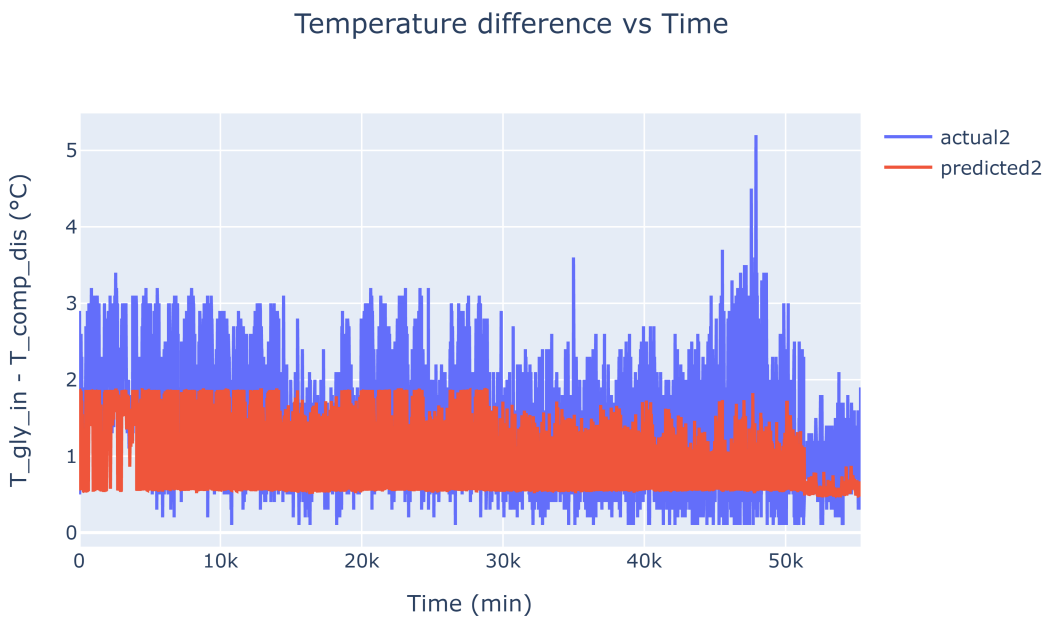

Figure 5.6: comparison of the actual and predicted temperature difference between the glycol inlet temperature and compressor discharge temperature over a time period after filtering out the negative values

the data were used to develop two equations. For low-speed, the equation had a maximum percentage error of 6.3%, while it was around 50% for the high-speed equation. Further analysis concluded that the equation was suitable for air-cooler cooling capacity prediction, while it was not suitable for dry coolers. Hence, various equations were used to check the accuracy of predicting the cooling capacity. Equation 5.3 resulted in more accurate results than equation 5.2. The average percentage deviation was 2.39% while the maximum percentage deviation was more than 11.63%. Figure 5.7 shows the validation curve, that is the difference between predicted and supplier-provided values. The validation curve proves that the equation fits closely with the supplier-provided data for cooling capacities.

$$C_{cond} = k_1 \cdot (T_{gly,in} - DBT) \cdot (FS\%)^{n_1} + k_2 \cdot (T_{gly,out} - DBT) \cdot (FS\%)^{n_1} + k_3 \tag{5.3}$$

To improve the accuracy of the equation 5.3, the equation was further divided based on high-speed (greater than 20% of the maximum speed) and low-speed data (lower than 20% of the maximum speed). The coefficients (k_1, k_2, k_3, and n_1) of the equation at high speed are 8.37, 140.2, 74.84, and 1.09 respectively. While the coefficients at low speeds are 86.3, 50.96, -5.14, and 1.04 respectively. The average error percentage for the equations were 2.2% and 0.45% respectively.

Wet-mode model

The model for the cooler in wet mode was developed in a similar way as described in section 3.2.2 and the glycol mass flow rate was assumed to be constant. But the deviation in predicted and actual cooling capacity during validation was quite high when equations 2.3 to 2.7 were used. So, the exponent of equations 2.3 and 2.4 were recalculated using the supplier data. Using the new exponents the predicted and actual cooling capacity was compared again. But still, the error in validation was quite large. So, the equation was further modified to fit the supplier data. Equations 2.3 to 2.6 were modified into a single equation 5.4.

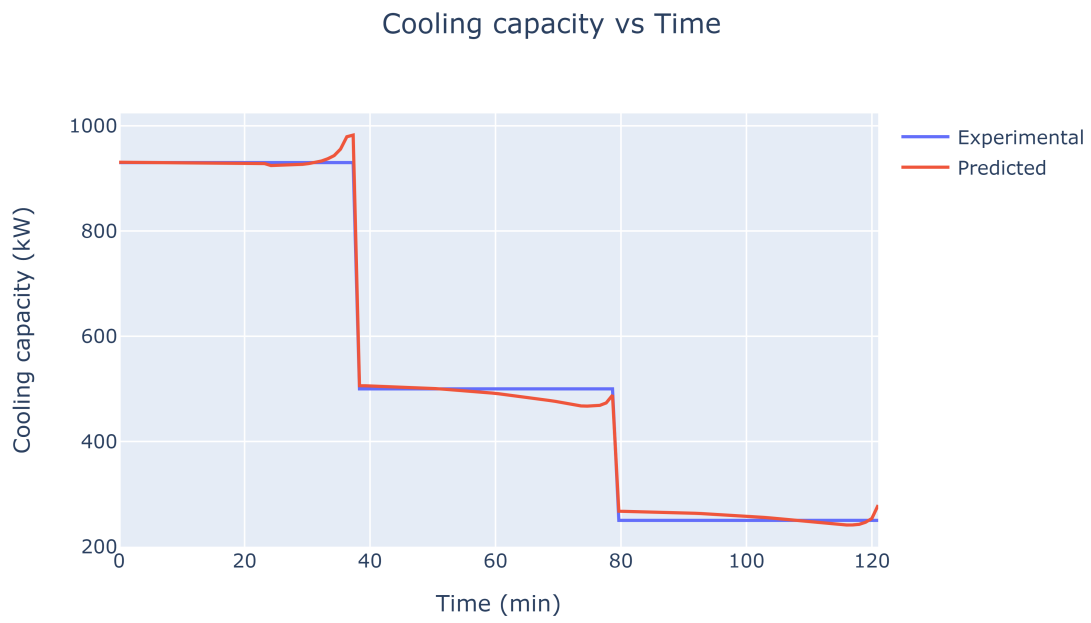

Figure 5.7: comparison of the predicted and supplier-provided cooling capacity of the hybrid cooler over a time period

$$C_{cond,nom,curr} = \left(\frac{k_1 \cdot (FS\%)^{n_1} \cdot C_{cond,nom}}{cf} \right) + k_2 \tag{5.4}$$

The coefficients k_1, k_2, and n_1 were calculated using the supplier data such that the validation error was minimum. The coefficients were calculated as 1.8, -679.32, and 0.358 respectively. The average and maximum error percentage for the equation was 0.33% and 13.09% respectively.

Combined model

A combination of both models was used to predict the cooling capacity of the cooler. For the GIST plant, the cooler fan speed is not measured. So, an operating condition was assumed for which the cooler fan could run at full speed. The cooler fan was assumed to run at full speed when the temperature difference between the cooler glycol outlet temperature set point and actual glycol outlet temperature is greater than 2°C. Using this assumption cooling capacities were predicted for the actual data. However, the deviation in actual and predicted cooling capacity was large. Further investigation showed that the equations used for the models do not cover the entire range of operating conditions due to a lack of supplier data. Moreover, the calculations were performed assuming a constant glycol mass flow rate but in the actual plant, the glycol mass flow rate is varying. But there is no glycol mass flow rate measurement for these coolers, so a correction for variation in glycol mass flow rate was not possible. Hence, machine learning techniques were used to check the possibility of modeling.

5.4.2. Cooler model using machine learning techniques

Since the empirical models could not predict cooling capacity for many operating conditions, especially for the wet condition of the cooler, machine-learning models were developed to predict the cooling capacity. As per the literature study (Sahoo (2023)), ANN (Artificial Neural Network) is the

most widely used model for performance prediction of the equipment. However, due to the unavailability of an extensive data set of the cooler, other machine-learning models were developed. The machine learning model was developed using four different methods: random forest, polynomial regression, SVR (Support Vector Regression), and GBR (Gradient Boosting Regression). These methods were chosen because these regression machine-learning models have been shown to be effective in predicting complex systems. The model was trained using data (cooler fan speed, cooler fan power consumption, cooling capacity, and the temperature difference between ambient temperature and outlet glycol temperature) from the cooler and validated using a separate test dataset. These data were provided by the cooler supplier and the supplier has performed calculations assuming a constant glycol mass flow rate. The validation process of the model involved comparing the predicted values of the model with the actual values from the test dataset.
For machine-learning model validation, MSE (Mean Square Error) and R^2 values are compared to check which model is the best for the given data set. Table 5.1 compares the MSE and R^2 values for all four models. It was observed from figure 5.8 that GBR technique had the lowest error as the predicted and actual cooling capacity matched well, hence, it was used to predict the cooler capacity and cooler fan power from the actual plant data.
However, as explained earlier for the GIST plant, the cooler fan speed was not measured. Hence,

Table 5.1: Summary of input & output parameters to be used for thesis

Model	**MSE (kW^2)**	**R^2**
Random forest	1349.93	0.9863
Polynomial regression	3072.86	0.9856
SVR	55052.82	0.1929
GBR	110.08	0.9984

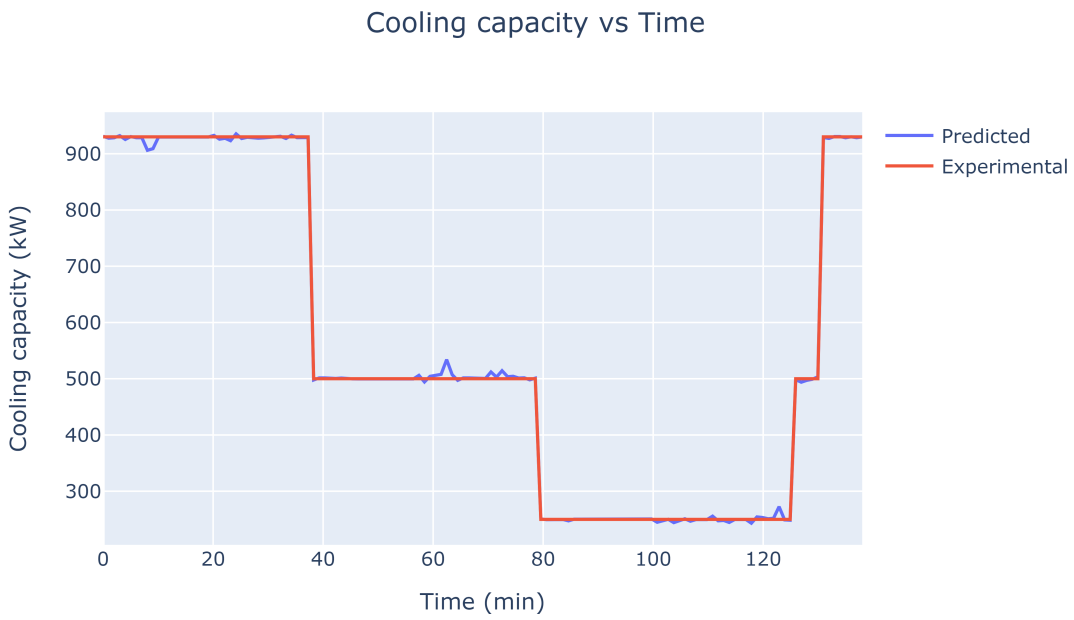

Figure 5.8: comparison of the predicted and supplier-provided cooling capacity of the hybrid cooler using GBR over a time period

using the same assumption and the actual plant data, the cooling capacity and cooler fan power were predicted. However, there was a huge deviation between the predicted and the actual data. Further investigation showed that the data used for training the model was not enough to cover the entire range of operations. Especially, there was no data where the fan speed was 100%. Moreover, the glycol mass flow rate correction could not be applied for the same reason which could be the reason for the deviation. Hence, it was concluded that both the empirical model and the machine learning model cannot be used for this plant as the supplier data does not cover the entire range of operations.

5.5. Air-cooler model

Air-cooler models were developed first using the supplier's data. But there was a deviation in the cooling capacity of the evaporators with respect to the cooling capacity predicted by the compressor model. Hence, the cooling capacities were calculated using the measured data from the plant and compared with the previously predicted cooling capacities (from the compressor model). Following subsections discuss the models and results in detail.

5.5.1. Air-cooler model using supplier's data

Supplier data (cooling capacity, glycol mass flow rate (constant), inlet air temperature, and inlet glycol temperature) was used to develop an air-cooler model. The variation in temperature difference between inlet air and inlet glycol temperature with the cooling capacity was used to develop a linear regression model. When the model is input with temperature difference, it gives the cooling capacity of the air-cooler as output. Equation 5.5 refers to the air-cooler model to predict the cooling capacity of the evaporator. Two separate models were developed, one for the 100 kW type air coolers and the other for the 150 kW type air coolers. Validation of the model was performed and the RMS error was 1.9 kW and 2.74 kW respectively for the 100 kW and 150 kW models.

$$C_{evap} = k_1 \cdot (T_{air,in} - T_{gly,in}) + k_2 \tag{5.5}$$

After the model validation, the model was used to predict the cooling capacity of the air coolers based on the actual plant data. Figure 5.9 refers to the cooling capacities of the air coolers predicted by the air-cooler DT. There were a lot of data points for which the cooling capacities were unusually high. Hence, further investigation was performed to understand the root cause and deviation was observed in the air temperature sensor reading. Figures 5.10 and 5.11 refer to the air temperature measured by the temperature sensors in the cold stores 4 and 7 respectively. Due to incorrect temperature measurement by the sensor, the prediction of cooling capacity by the air cooler model was inaccurate. So, the part of the data which had accurate measurements were used for further analysis.

Figure 5.12 shows the comparison of cooling capacities predicted by the compressor model and the air-cooler model. The reason for this could be the assumption of a constant glycol mass flow rate. Hence, the cooling capacity was corrected for the actual glycol mass flow rate. As described in section 5.2, the cooling capacity varies proportionally to the glycol mass flow rate, so the cooling capacities predicted by the model were corrected in proportion to the actual glycol mass flow rate. However, the capacity predicted by the corrected air-cooler model was still higher than the compressor model, which implies the air-cooler is underperforming (not performing as per the manufacturer's design). This was concluded because the air-cooler model was based on the design data provided by the air-cooler manufacturer.

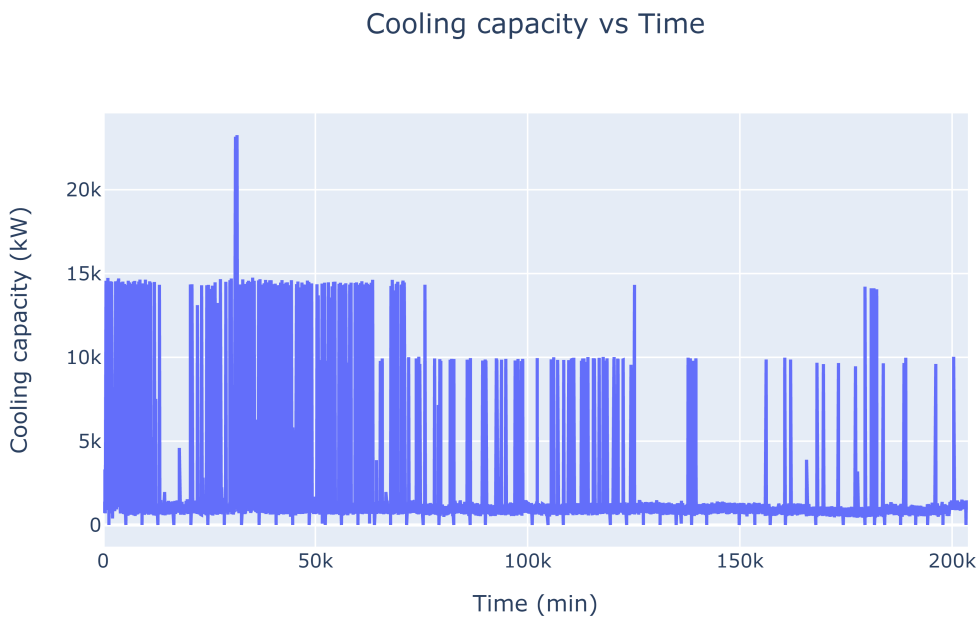

Figure 5.9: Predicted cooling capacity by the air-cooler model

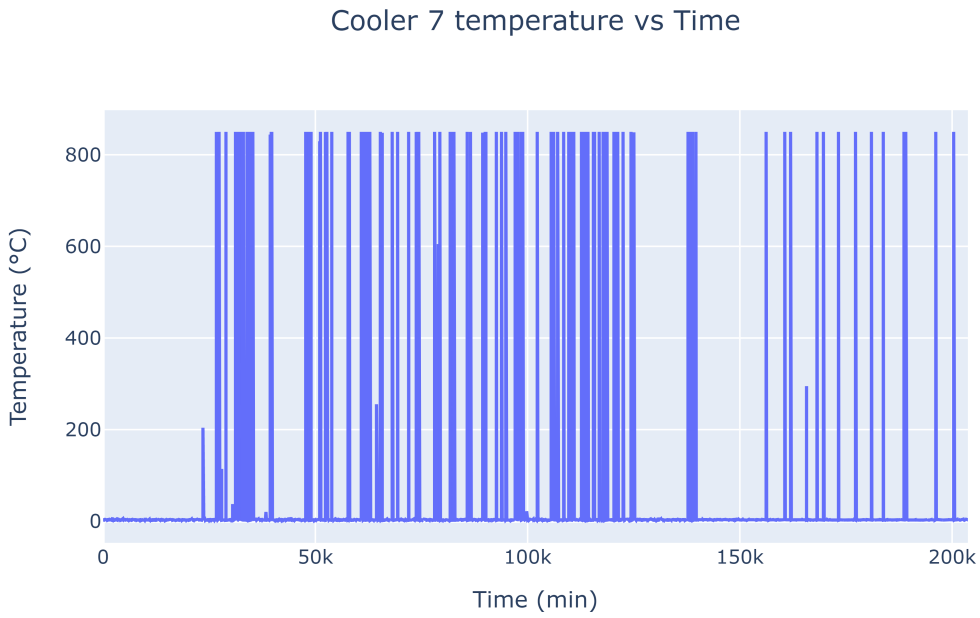

Figure 5.10: Air temperature measured by the sensor inside cold store 4

5.5.2. Air-cooler model using measured plant data

Further investigation was performed to verify the deviation in the performance of the air-coolers. In the GIST plant, inlet glycol temperature, outlet glycol temperature, and glycol volume flow rate are measured across the air coolers. The fluid used is 30% glycol, from which the specific heat capacity

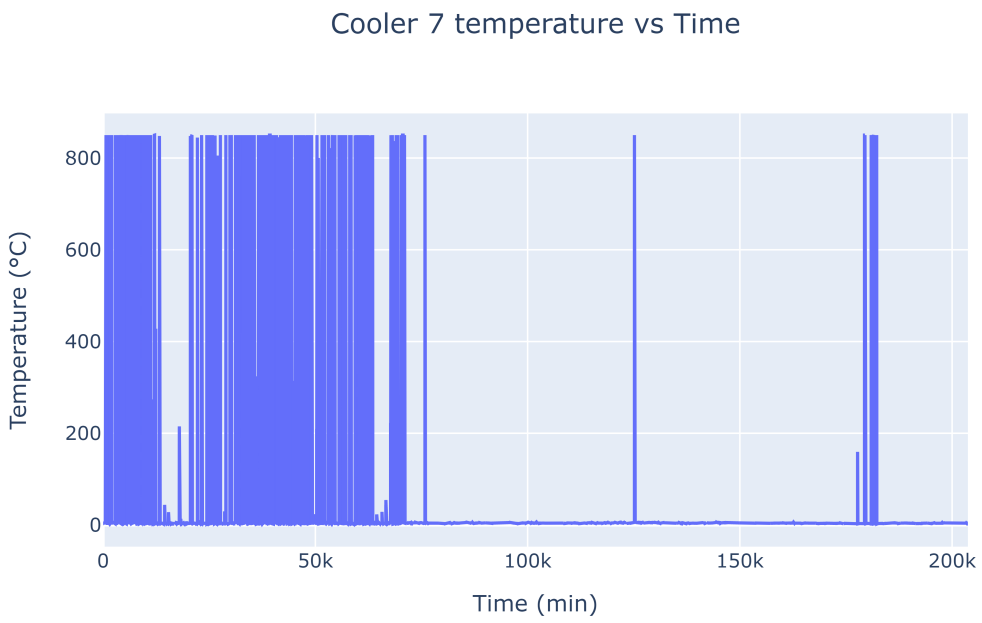

Figure 5.11: Air temperature measured by the sensor inside cold store 7

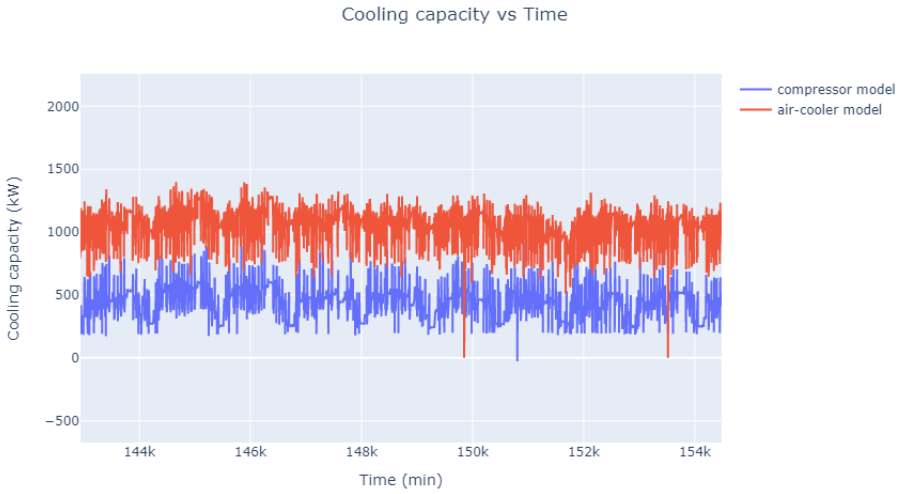

Figure 5.12: Comparison of cooling capacities between air cooler model and compressor model

was calculated. Based on these data, the cooling capacity of the air coolers was calculated. Equation 5.6 was used to calculate the cooling capacity of air coolers.

$$C_{aircooler} = \dot{m} \cdot cp \cdot (T_{gly,out} - T_{gly,in}) \tag{5.6}$$

Figure 5.13 refers to the comparison of the cooling capacities of air coolers predicted by the compressor model and the cooling capacity calculated from the measured plant data. The cooling capacity predicted by the compressor model and the one calculated from plant data were matching within an error margin of 8.9%, which was significantly lower than the mismatch in the air-cooler

model. Hence, the cooling capacities from the compressor model and the one calculated from the plant data correspond. This concludes that the design of the air coolers was not as per the specification provided by the manufacturer.

The deviation in the measured values and the compressor model could be due to the thermal en-

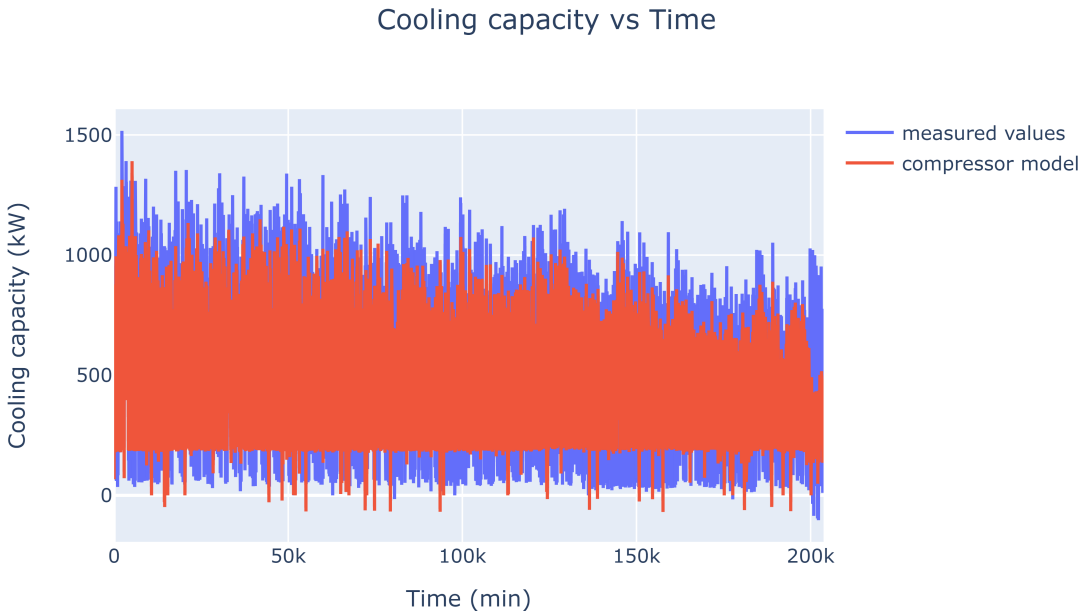

Figure 5.13: Comparison of measured cooling capacity and the cooling capacity predicted by the compressor model

ergy loss during the flow of the cold glycol from the chiller to the air cooler and due to the heat added by the pumps. However, it is difficult to quantify these energy losses, hence it is difficult to say if these losses alone account for the deviation in the air cooler performance.

5.6. Air-coolers optimization

Each air cooler is associated with a cold store. To optimize the air coolers there are various techniques. However, not all the techniques can be utilized in the GIST plant because of the limitation of the systems installed. One strategy that can be implemented is:

Optimal Defrosting: Developing an optimal scheduling strategy for defrost cycles across multiple cold stores is essential. This can improve the energy performance of the air coolers. Moreover, coordinating defrost cycles and maintenance tasks efficiently can reduce downtime, improve system performance, and minimize energy consumption.

5.6.1. Optimal defrosting

Hot glycol defrosting is used in the GIST plant to defrost the air coolers. Hot glycol defrosting is a common method used in refrigeration systems to remove ice or frost buildup from the evaporator coil. During normal operation, the evaporator coil of a refrigeration system gets cold, causing moisture in the air to condense and freeze on its surface. Over time, this ice buildup can reduce the efficiency of the system and hinder its ability to cool properly. Hot glycol defrosting is an efficient and effective technique to melt the ice and restore the optimal performance of the system.

The hot glycol defrosting process involves the use of high-temperature glycol from the system's chiller to heat up the evaporator coil. Here is a step-by-step explanation of the hot glycol defrosting cycle:

1. Initiation: The hot glycol defrosting cycle begins when the refrigeration system detects a predetermined amount of ice or frost buildup on the evaporator coil. This triggers a defrost cycle, temporarily interrupting the cooling process.
2. Hot glycol flow: The system's hot glycol is directed to the evaporator coil. This is achieved by closing the cooling valve which stops the flow of cold glycol into the evaporator and simultaneously opening the defrost valve which allows the flow of hot glycol into the evaporator.
3. Chiller operation: The chiller continues to operate during the defrost cycle, but its hot glycol goes to both the hybrid cooler and evaporator.
4. Heat transfer: The high-temperature glycol from the chiller enter the evaporator coil, which is cold due to the ice buildup. As the hot glycol flows through the coil, it transfers its heat energy to the coil's surface. This heat causes the ice to melt, converting it back into water.
5. Drainage: The melted ice or frost collects in a drain pan or a series of drains within the evaporator, where it is then directed out of the system through a drain line.
6. Termination: Once the ice has melted and the evaporator coil is clear, the hot glycol defrost cycle is terminated. The defrost valve is closed and the cooling valve is opened.
7. Resuming cooling operation: After the defrost cycle, the refrigeration system resumes its normal cooling operation. The evaporator coil is now free from ice or frost, allowing for efficient heat transfer and improved cooling performance.

Currently, the defrosting is controlled by a fixed time interval, that is after a fixed time period defrosting is switched ON and it remains ON for a fixed period of time and then it is switched OFF. This leads to excess energy consumption because the frost thickness may not be enough to start defrosting or the defrosting may be continued even after the defrosting is complete. Moreover, too many defrost cycles can have a negative effect on the food being preserved. Hence, to optimize the defrosting process it is important to calculate when the defrosting has to be started and the exact defrosting time.
Most of the defrosting techniques reported in the literature have used experimental (lab experiment) techniques to calculate the defrosting time. But in the running plant, it is not a viable option as it is difficult to set up the experimental setup. Hence, the analytical method should be used. The analytical method includes an energy balance model, where an energy balance between the air and glycol side is used to check the amount of frost accumulated. An adaptive defrosting technique has been developed by Danfoss (manufacturer) using the same technique. The energy balance model used for this technique is shown in figure 5.14. At the start of the process, that is when the evaporator is ice-free, an energy balance between the glycol side and air side is expected. But when the ice starts accumulating part of the energy goes to the formation of frost, hence, cooling capacity is reduced due to frost formation and obstruction of airflow. Once the cooling capacity reduces to a particular value, the defrosting is started. This technique should be used for the GIST plant. However, the energy model for the glycol side cannot be developed for the GIST plant as there is no temperature sensor at the outlet of the glycol flow.

5.7. Conclusion

In conclusion, the analysis of the GIST plant reveals several key findings:

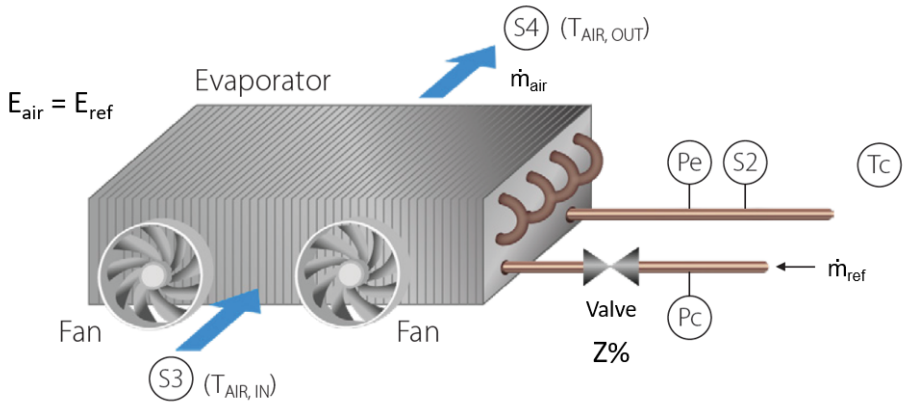

Figure 5.14: Energy model used for the defrosting model for air-coolers (Manufacturer - Danfoss)

- The two chillers operating in parallel are suboptimal, leading to approximately 2.5% excess energy consumption. The frequent starting and stopping of the second chiller may result in mechanical wear and tear.
- The evaporators of both chillers deviate from the design specifications, resulting in a total temperature difference of 1.29°C in the evaporating temperature. This discrepancy leads to 3-5% higher energy consumption compared to the intended design.
- Similarly, the condenser performance of both chillers deviates from the specified design, with a total temperature difference of 1.15°C in the condensing temperature. This variation causes an excess energy consumption of 3-5%. Additionally, multiple data points indicate a negative temperature difference between the glycol inlet temperature and saturated discharge temperature, confirming the frequent starts and stops of the chiller.
- Despite the development of a hybrid cooler model using empirical and data-driven approaches, neither model accurately predicts the condensing capacity due to incomplete data coverage across all operational ranges.
- The air cooler model predicts significantly higher cooling capacities than the compressor model, which is theoretically impossible. Further investigation reveals that temperature sensors for cold stores 4 and 7 are not functioning correctly, leading to inaccuracies in predicted capacities. The air cooler underperforms according to the supplier's specifications. Consequently, cooling capacities were calculated using measured plant data, reinforcing the conclusion of underperformance. Furthermore, a cooling capacity deviation is observed between the cooling capacity from the measured plant data and the compressor model, likely due to heat added during the flow of cold glycol from the chiller to the air coolers and the heat added by the pumps.
- The evaluation of the GIST plant identifies two faults: the control algorithm of the chillers and the temperature sensors of cold stores 4 and 7. Additionally, certain equipment, such as the chiller evaporators, condensers, and air coolers, does not meet design or supplier specifications. Rectifying these faults and implementing design modifications can lead to improvements in energy performance and maintenance savings.
- The optimization of parallel chiller operation can achieve energy savings of 2.42%. Design modifications targeting air coolers, evaporators, and condensers can potentially yield estimated energy savings of 8-10%. Although the energy savings from adaptive defrosting optimization are difficult to quantify due to limited data availability, it can contribute to energy

conservation. The hybrid cooler also has the potential for energy savings, but reliable data is currently unavailable for accurate calculations.

- By implementing these optimizations and design modifications, the GIST plant can achieve a total energy savings of approximately 170 MWh, resulting in annual electricity cost savings of $ 70,000. Furthermore, these measures can help mitigate the release of approximately 60 tonnes of CO_2 into the atmosphere, contributing to a reduction in carbon footprint and the alleviation of global warming.

6

Conclusion

This research aimed to optimize the energy performance of refrigeration systems in order to reduce energy consumption, minimize greenhouse gas emissions, and contribute to a more sustainable future. The research objectives were successfully achieved through the development of digital twins (DTs) for equipment modeling, evaluation of energy performance, identification of deviations, and implementation of optimization strategies.

The research highlighted the significance of refrigeration systems in global energy consumption, particularly in the food & beverage industry, and their contribution to CO_2 emissions. The need to address sub-optimal operation and inadequate performance of refrigeration systems was emphasized, considering the adverse effects of greenhouse gas emissions and global warming.

The research objectives of developing and evaluating digital twins (DTs) for each type of equipment, analyzing their energy performance, comparing them with actual site data, identifying and correcting deviations, optimizing system set points and defrosting, and calculating energy savings have been successfully addressed through the study of three plants: Verkade Plant, LST Plant, and GIST Plant.

For the Verkade Plant, it was concluded that the DT models developed were accurate within a 5% error margin, providing reliable results for equipment analysis. The optimization of the plant led to significant energy savings of 7% annually, amounting to approximately 32 MWh of electrical energy, $ 13,000 in cost savings, and 11 tonnes of CO_2 reduction per year. These energy savings contribute to mitigating the effects of global warming and align with the goals of the Paris Agreement.

In the case of the LST Plant, various equipment inefficiencies were identified. The screw compressors were found to be operating suboptimally, leading to imbalanced load sharing, increased energy consumption, mechanical wear, and higher maintenance frequency. The evaporative condenser exhibited signs of refrigerant leakage, and the control of the expansion valve opening and the feed control valve for freeze dryers were unstable. The energy savings strategies proposed for the LST Plant included optimizing the parallel operation of screw compressors (1.55% energy savings), adjusting the condensing temperature set point (11.06% energy savings), and rectifying the evaporator feed valve control. These optimizations could save approximately 200 MWh of energy annually, resulting in $ 81,000 in electricity cost savings and preventing the release of 70 tonnes of CO_2 into the atmosphere. Such reductions in CO_2 emissions align with the goals of the Paris Agreement and contribute to mitigating global warming.

The analysis of the GIST plant revealed equipment inefficiencies, including suboptimal parallel chiller operation, deviations in evaporators and condensers from design specifications, and inaccurate temperature sensors. Faults were identified in the control algorithm and temperature sensors. Proposed optimizations included parallel chiller operation (2.42% energy savings), design modifi-

cations (estimated 8-10% energy savings), and adaptive defrosting. Implementing these measures could save 170 MWh of energy annually, reducing electricity costs by $70,000 and preventing the release of 60 tonnes of CO_2, aligning with the Paris Agreement and mitigating global warming.
In conclusion, the research objectives were successfully achieved by developing accurate DT models, evaluating energy performance, identifying deviations, and implementing energy-saving measures in all three plants: the Verkade, LST, and GIST plants. The findings highlight the potential for significant energy and cost savings, as well as substantial CO_2 emission reductions.
However, there are some limitations in the research which can be overcome by further research. Some equipment models could not be developed and some models could not be validated due to the lack of experimental data and actual plant data respectively. More sensors could be installed in the plant to get relevant information to try new energy savings strategies. There were few performances of equipment that could not be explained in the current study. Those can be analyzed in further studies.
Further studies are warranted to explore additional optimization opportunities, such as the correction of the evaporator feed valve control and defrosting, which was challenging to quantify in terms of energy savings. Additionally, the research can be extended to analyze more plants and validate the applicability of the DT models and energy-saving strategies in different settings. Continuous monitoring and analysis of energy performance in various industrial plants can contribute to achieving sustainability goals and further refining the optimization techniques for improved energy efficiency.

Bibliography

Ahmed, R., Mahadzir, S., Rozali, N. E. M., Biswas, K., Matovu, F., & Ahmed, K. (2021). Artificial intelligence techniques in refrigeration system modelling and optimization: A multi-disciplinary review. *Sustainable Energy Technologies and Assessments*, *47*, 101488.

Barricelli, B. R., Casiraghi, E., & Fogli, D. (2019). A survey on digital twin: Definitions, characteristics, applications, and design implications. *IEEE access*, *7*, 167653–167671.

Belman-Flores, J., Mota-Babiloni, A., Ledesma, S., & Makhnatch, P. (2017). Using anns to approach to the energy performance for a small refrigeration system working with r134a and two alternative lower gwp mixtures. *Applied Thermal Engineering*, *127*, 996–1004.

Berglöf, K. (2013). Experience from energy optimisation in refrigeration and air-conditioning plants through field measurements. *Compressors, 8th international conference*.

Breiman, L. (2001). Random forests. *Machine learning*, *45*, 5–32.

Cho, H., Ryu, C., Kim, Y., & Kim, H. Y. (2005). Effects of refrigerant charge amount on the performance of a transcritical co2 heat pump. *International Journal of Refrigeration*, *28*(8), 1266–1273.

Choi, J., & Kim, Y. C. (2002). The effects of improper refrigerant charge on the performance of a heat pump with an electronic expansion valve and capillary tube. *Energy*, *27*(4), 391–404.

Cobo, M., & Renilla, R. (2015). Development and dissemination of cost-effective strategies to improve energy-efficiency in cooling systems in the food and drink sector. *Institut International du Froid - International Institute of Refrigeration, France*.

Dincer, I., Rosen, M. A., & Ahmadi, P. (2017). *Optimization of energy systems*. John Wiley & Sons.

Draper, N. (1966). Polynomial regression in the case of errors in the variables. *Technometrics*, *8(3)*, 499–509.

Farzad, M. (1990). *Modeling the effects of refrigerant charging on air conditioner performance characteristics for three expansion devices*. Texas A&M University.

Food & Drink Federation, Institute of Refrigeration, & British Beer & Pub Association. (2007). *Food & drink industry refrigeration efficiency initiative*. Retrieved June 6, 2023, from http://www.cold.org.gr/library/downloads/Docs/Improving%5C%20refrigeration%5C%20system%5C%20efficiency_Guidance.pdf

Friedman, J. H. (2001). Greedy function approximation: A gradient boosting machine. *Annals of statistics*, 1189–1232.

Goswami, D., Ek, G., Leung, M., Jotshi, C., Sherif, S., & Colacino, F. (1997). Effect of refrigerant charge on the performance of air-conditioning systems. *IECEC-97 Proceedings of the Thirty-Second Intersociety Energy Conversion Engineering Conference (Cat. No. 97CH6203)*, *3*, 1635–1640.

Grace, I., Datta, D., & Tassou, S. (2005). Sensitivity of refrigeration system performance to charge levels and parameters for on-line leak detection. *Applied Thermal Engineering*, *25*(4), 557–566.

Grimmelius, H., Woud, J. K., & Been, G. (1995). On-line failure diagnosis for compression refrigeration plants. *International Journal of Refrigeration*, *18*(1), 31–41.

Gurubalan, A., Maiya, M., & Geoghegan, P. J. (2019). A comprehensive review of liquid desiccant air conditioning system. *Applied Energy*, *254*, 113673.

Helm, J. M., Swiergosz, A. M., Haeberle, H. S., Karnuta, J. M., Schaffer, J. L., Krebs, V. E., Spitzer, A. I., & Ramkumar, P. N. (2020). Machine learning and artificial intelligence: Definitions,

applications, and future directions. *Current reviews in musculoskeletal medicine*, *13*(1), 69–76.

Kiritsis, D. (2011). Closed-loop plm for intelligent products in the era of the internet of things. *Computer-Aided Design*, *43*(5), 479–501.

Manske, K., Reindl, D., & Klein, S. (2001). Evaporative condenser control in industrial refrigeration systems. *International journal of refrigeration*, *24*(7), 676–691.

McMullan, J. T. (2002). Refrigeration and the environmentissues and strategies for the future. *International journal of refrigeration*, *25*(1), 89–99.

Moran, P., Goggins, J., & Hajdukiewicz, M. (2017). Super-insulate or use renewable technology? life cycle cost, energy and global warming potential analysis of nearly zero energy buildings (nzeb) in a temperate oceanic climate. *Energy and Buildings*, *139*, 590–607.

Ntagkras, D. (2022). Creation of digital twin for fault detection and optimization of refrigeration plants. *Internship report, Mechanical Engineering, Delft University of Technology*.

Outlook, B. E. (2019). 2019 edition. *London, United Kingdom2019*.

Pearson, A. (2019). Continuous monitoring of energy performance in industrial systems. *25th IIR International Congress of Refrigeration Proceedings*.

Prakash, J. A. M. (2006). Energy optimisation potential through improved onsite analysing methods in refrigeration. *Master of Science Thesis, Department of Energy Technology, Royal Institute of Technology, Stockholm, Sweden*.

Rios, J., Hernandez, J. C., Oliva, M., & Mas, F. (2015). Product avatar as digital counterpart of a physical individual product: Literature review and implications in an aircraft. *Transdisciplinary Lifecycle Analysis of Systems*, 657–666.

Sahoo, A. (2023). Optimizing the energy performance of industrial refrigeration plants using digital twins. *Literature study, Mechanical Engineering, Delft University of Technology*.

Smola, A. J., & Schölkopf, B. (2004). A tutorial on support vector regression. *Statistics and computing*, *14*, 199–222.

Solomon, S., Qin, D., Manning, M., Chen, Z., Marquis, M., Averyt, K., Tignor, M., & Miller, H. (2007). Ipcc fourth assessment report (ar4). *Climate change*, *374*.

Tao, F., Zhang, H., Liu, A., & Nee, A. Y. (2018). Digital twin in industry: State-of-the-art. *IEEE Transactions on industrial informatics*, *15*(4), 2405–2415.

Tassou, S., & Grace, I. (2005). Fault diagnosis and refrigerant leak detection in vapour compression refrigeration systems. *International journal of refrigeration*, *28*(5), 680–688.

United Nations. (2018). *The potential to improve the energy efficiency of refrigeration, air-conditioning and heat pumps*. Retrieved June 6, 2023, from https://ozone.unep.org/sites/default/files/2019-08/briefingnote-b_potential-to-improve-the-energy-efficiency-of-refrigeration-air-conditioning-and-heat-pumps.pdf